Developmental roles of Auxin Binding Protein 1 in *Arabidopsis thaliana*

Zuzana Gelová [a], Michelle Gallei [a], Markéta Pernisová [b,c], Géraldine Brunoud [b], Xixi Zhang [a,d], Matouš Glanc [a,e], Lanxin Li [a], Jaroslav Michalko [a], Zlata Pavlovičová [a], Inge Verstraeten [a], Huibin Han [a], Jakub Hajný [a,f], Robert Hauschild [a], Milada Čovanová [g], Marta Zwiewka [h], Lukas Hoermayer [a], Matyáš Fendrych [a], Tongda Xu [i], Teva Vernoux [b], Jiří Friml [a,*]

[a] *Institute of Science and Technology (IST), Am Campus 1, 3400 Klosterneuburg, Austria*
[b] *Laboratoire Reproduction et Développement des Plantes, Univ Lyon, ENS de Lyon, UCB Lyon 1, CNRS, INRA, 69342 Lyon, France*
[c] *Functional Genomics and Proteomics, National Centre for Biomolecular Research, Faculty of Science, Masaryk University, Kamenice 5, 62500 Brno, Czech Republic*
[d] *Department of Applied Genetics and Cell Biology, University of Natural Resources and Life Sciences (BOKU), Muthgasse 18, 1190 Vienna, Austria*
[e] *Department of Experimental Plant Biology, Faculty of Science, Charles University, Viničná 5, 12844 Prague, Czech Republic*
[f] *Laboratory of Growth Regulators, The Czech Academy of Sciences, Institute of Experimental Botany & Palacký University, Šlechtitelů 27, 78371 Olomouc, Czech Republic*
[g] *The Czech Academy of Sciences, Institute of Experimental Botany, Rozvojová 263, 165 02 Praha 6, Czech Republic*
[h] *Mendel Centre for Plant Genomics and Proteomics, Central European Institute of Technology (CEITEC), Masaryk University, Kamenice 5, 625 00 Brno, Czech Republic*
[i] *FAFU-Joint Centre, Horticulture and Metabolic Biology Centre, Haixia Institute of Science and Technology, Fujian Agriculture and Forestry University, Fuzhou, 350002 Fujian, People's Republic of China*

ARTICLE INFO

ABSTRACT

Auxin is a major plant growth regulator, but current models on auxin perception and signaling cannot explain the whole plethora of auxin effects, in particular those associated with rapid responses. A possible candidate for a component of additional auxin perception mechanisms is the *AUXIN BINDING PROTEIN 1 (ABP1)*, whose function *in planta* remains unclear.

Here we combined expression analysis with gain- and loss-of-function approaches to analyze the role of *ABP1* in plant development. *ABP1* shows a broad expression largely overlapping with, but not regulated by, transcriptional auxin response activity. Furthermore, *ABP1* activity is not essential for the transcriptional auxin signaling. Genetic *in planta* analysis revealed that *abp1* loss-of-function mutants show largely normal development with minor defects in bolting. On the other hand, *ABP1* gain-of-function alleles show a broad range of growth and developmental defects, including root and hypocotyl growth and bending, lateral root and leaf development, bolting, as well as response to heat stress. At the cellular level, *ABP1* gain-of-function leads to impaired auxin effect on PIN polar distribution and affects BFA-sensitive PIN intracellular aggregation.

The gain-of-function analysis suggests a broad, but still mechanistically unclear involvement of *ABP1* in plant development, possibly masked in *abp1* loss-of-function mutants by a functional redundancy.

1. Introduction

The phytohormone auxin is a major coordinator of plant growth that governs a multitude of developmental processes. Its versatility is related to its differential distribution within plant tissues and the ability of cellular auxin concentrations determine various cell fate decisions. The establishment of these morphogenic auxin gradients and local auxin maxima is achieved by a combination of local auxin biosynthesis [1] and synergetic, directional cell-to-cell polar auxin transport [2].

Auxin concentration affects cellular processes, mainly through a modulation of transcription. A broad range of auxin-responsive transcriptional regulators remodel the transcriptome of cells through tissue specific expression and thus trigger complex developmental changes [3]. On this transcriptional level, auxin controls processes such as embryogenesis, vascular tissues formation and organogenesis of the shoot apex or maintenance of the root apical meristem [4].

Nevertheless, some cellular auxin effects occur too fast to be a result of transcriptome remodeling and/or they were shown not to require

---

functional transcription or *de novo* protein synthesis. Auxin triggers rapid hyperpolarization of the plasma membrane leading to protoplast swelling [5,6], induces calcium ion and proton fluxes across the plasma membrane and therefore alkalizes the apoplast [7,8], and inhibits clathrin-mediated endocytic trafficking processes [9,10].

The auxin signal is transduced via several mechanisms [11,12]. The canonical pathway is mediated by a nuclear-localized co-receptor complex comprising the TRANSPORT INHIBITOR RESISTANT1/AUXIN SIGNALING F-BOX (TIR1/AFB) F-box proteins and the AUXIN/INDOLE-3-ACETIC ACID (Aux/IAA) transcriptional repressors. Here, auxin promotes the interaction of TIR1/AFBs with Aux/IAAs that results in ubiquitin-dependent degradation of the Aux/IAA proteins. Aux/IAA proteins act as transcriptional repressors of AUXIN RESPONSE FACTORs (ARFs) transcription factors and thus their degradation activates auxin-responsive transcription [13].

Notably, recent findings suggest that TIR1/AFB signaling mediates both rapid transcriptional as well as even faster non-transcriptional auxin effects on growth. In shoots, auxin via the TIR1/AFB pathway induces fast apoplast acidification and growth promotion by a rapid transcriptional regulation of *SMALL AUXIN UPREGULATED (SAUR)* genes [14,15]. In contrast, auxin-mediated growth inhibition in roots occurs within 30 s and does not require *de novo* protein synthesis but is still strictly dependent on the TIR1/AFB pathway [16]. Furthermore, the auxin-mediated fast depolarization of the plasma membrane and Ca^{2+} uptake were demonstrably linked with the TIR1/AFB signaling pathway [17].

Recently, two additional non-canonical auxin-sensing mechanisms were described. Auxin has been shown to bind directly to the atypical ARF ARF3/ETTIN to modulate chromatin states and interaction with other transcriptional regulators during gynoecium development [18, 19]. The other mechanism involves TRANSMEMBRANE KINASE 1 (TMK1), a member of the plasma membrane-localized TMK receptor-like kinase family [20]. It was shown that auxin triggers cleavage of TMK1's intracellular kinase domain and its consequent translocation to the nucleus. There, the TMK1 kinase domain binds, phosphorylates and thus stabilizes two non-canonical Aux/IAAs, IAA32 and IAA34. Via this alternative transcriptional pathway, auxin regulates apical hook development [21]. TMK1 also regulates lateral root organogenesis and auxin biosynthesis by other cellular mechanisms [22,23]. Importantly, while the canonical TIR1/AFB receptors sense auxin predominantly in the nucleus, the TMKs located in the plasma membrane may perceive auxin from the apoplast by an unknown perception mechanism.

The accumulating developmental roles of TMKs in conjunction with their plasma membrane localization stir up a decades-lasting debate on the existence of a cell-surface auxin receptor. In the past, the best candidate appeared to be AUXIN BINDING PROTEIN 1 (ABP1). This evolutionarily conserved 22-kDa glycoprotein [24,25] has been shown to bind auxin at apoplastic pH 5.5 [26–28] and although it predominantly localizes to the endoplasmic reticulum (ER), a small fraction has been proposed to reside in the apoplast [29]. ABP1 has been proposed to be mainly associated with rapid non-transcriptional auxin-mediated processes, but the genetic analysis has been hampered by the lack of viable loss-of-function mutants. It has also remained unclear how apoplastic ABP1 could transduce the auxin signal into the cell and therefore the requirement of a plasma membrane-localized docking partner was hypothesized. Later, ABP1 was found to interact with TMK1 in an auxin-dependent manner. It was proposed that ABP1 and TMK1 form an auxin-sensing complex at the plasma membrane that activates downstream cellular processes via small GTPases ROP2 and ROP6 and their effector proteins RIC1 and RIC4 [30–32]. Based on the phenotypes of *ABP1* gain-of-function mutants, the weak *abp1-5* allele and conditional *abp1* knock-down lines [33] *ABP1* was proposed to play a role in clathrin-mediated endocytosis [10,34,35], growth-correlating microtubule re-orientation [36], cell wall remodeling [37] or interdigitated growth of leaf pavement cells [30,36]. All these proposed roles were

called into question by the failure to complement the alleged embryo lethal *abp1* phenotypes, by the coding sequence of *ABP1* [35] and by the identification of new *abp1* knock-out alleles with no obvious morphological phenotypes [38]. These discrepancies were clarified by proofs that the original *abp1* embryo lethal phenotypes were caused by disruption of a neighboring gene rather than *ABP1* itself [39,40]. Furthermore, the *abp1-5* line carries many additional mutations [41] and the conditional knock-down lines, despite independently targeting either ABP1 mRNA or protein [33], also have other targets [42]. Thus, with much of the previously used genetic material called into question and with only superficial phenotype analysis of the more recent, verified knock-out lines [38], the developmental and physiological roles of ABP1 still remain largely unclear.

Here we used the verified gain- and loss-of-function mutant lines in Arabidopsis to (re)evaluate the role of ABP1 in cellular processes, physiological responses and plant development.

2. Materials and methods

2.1. Plant material

Wild-type Col-0 (NASC, The Nottingham Arabidopsis Stock Centre; http://www.arabidopsis.info, N1092) was used as a control line. Previously published *Arabidopsis thaliana* lines were used in this study: *ABP1$_{i1,2}$::GUS* [43]; *abp1-C1*, *abp1-TD1* and background Col-0 used for generating *abp1-C1* by CRISPR (in text mentioned as WT for *abp1-C1*) [38]; *DR5rev::GFP* [44]; *35S::ABP1-GFP* [10]. The following *Arabidopsis thaliana* lines were generated in this study: *DR5rev::GFP;abp1-C1* and *DR5rev::GFP;abp1-TD1*. *DR5rev::GFP* was introduced into both *abp1* mutant backgrounds by genetic crossing. The *ABP1::ABP1;abp1-TD1* line was generated by introducing the *ABP1::ABP1* construct into the *abp1-TD1* background and the *ABP1::GFP-ABP1;abp1-C1* line was generated by introducing the *ABP1::GFP-ABP1* construct into the *abp1-C1* background using Agrobacterium-mediated transformation [45]. All transgenic lines and mutants used in this study are listed in Supplemental Table 1. All primers used for genotyping are listed in Supplemental Table 2.

2.2. Vector construction

All plasmids were constructed by the Gateway cloning technology (www.invitrogen.com). Previously generated constructs pDONR221-ABP1cDNA and pDONR221-ABP1cDNA-M2X containing cDNA sequence of *ABP1* [35] were used to construct the final plasmids *35S::ABP1* and *35S::ABP1-M2X* by recombination into the p2GW7 destination vector. *ABP1::ABP1* was constructed as follows: the 3.0 kb promoter, genomic coding region and 0.6 kb of 3' untranslated region for *ABP1* was amplified and inserted into a pDONR-Zeo vector, then inserted into the pGWB401 destination vector. *ABP1::GFP-ABP1* was constructed using a 1585 bp promoter fragment [43] and a N-terminal GFP fusion directly after the N-terminal signal peptide. The GFP insertion was flanked at the 5' end by a PKAPA linker (tested for cleavage using the SignalP-5.0 server) and at the 3' end by a PKPAPKPA linker. The *ABP1* fragments were amplified from genomic DNA using primer pairs 1 and 2 (promoter, signal peptide and 5' linker), 3 and 4 (GFP and 3' linker) and 5 and 6 (gABP1 gene body including 3' UTR). All three fragments were fused in a single overlap PCR reaction and cloned into the pDONR221 entry vector. The resulting construct was cloned into the pKGW,0 destination vector and sequenced. All primers used in this study are listed in Supplemental Table 2. All plasmids used in this study are listed in Supplemental Table 3.

2.3. Growth conditions

Seeds were chlorine gas sterilized or sterilized with 70 % EtOH, sown on plates with ½ Murashige and Skoog (MS) medium supplemented with

1 % (w/v) sucrose and 0.8 % (w/v) Phytoagar (pH 5.9) and stratified for 2 days at 4 °C. For experiments using Arabidopsis seedlings, the seedlings were grown on plates at 21 °C under a long-day photoperiod (16 h light/8 h dark) for the required time period. For experiments performed in soil, *in vitro* grown seedlings were transferred to soil and grown under a long-day photoperiod (16 h light/8 h dark) at 21 °C and 40 % relative humidity for the required time period. The light sources used were Philips GreenPower light emitting diode production modules in a deep red, far red, blue combination with a photon density of 140.4 μmol/m^2/s ± 3 %. For phyllotaxis measurement experiment, plants in soil were cultivated in growth chambers at 22 °C and 40 % relative humidity. Plants were kept under short day conditions (8 h light/16 h dark) for 28 days and then transferred to long day conditions (16 h light/8 h dark). Plants were always grown together within the growth chamber and with randomized positions within each tray in order to minimize the effect of environmental fluctuations. For etiolated growth, the plated and stratified seeds were exposed to light for 8 h and further covered with aluminum foil to cultivate them in the dark at 21 °C for 4 days (the shoot gravity response experiment) or in the dark chamber at 24 °C for 5 days (the etiolated growth experiment).

2.4. Histochemical GUS staining

6-d-old light-grown seedlings or 3-d-old etiolated seedlings of *ABP1$_{i1,2}$::GUS* were stained in 0.1 M sodium phosphate buffer (pH 7.0) containing 0.1 % X-GlcA sodium salt (Duchefa, 7240-90-6), 2 mM K$_3$[Fe (CN)$_6$], 2 mM K$_4$[Fe(CN)$_6$] and 0.05 % Triton X-100 for 2 h (light-grown seedlings) or 1 h (etiolated seedlings) at 37 °C. Further, samples were incubated overnight in 80 % (v/v) ethanol at room temperature. Tissue clearing was conducted as previously described [46]. DIC microscopy for analysis of GUS staining was performed using an Olympus BX53 microscope equipped with 10x and 20x air objectives and a DP26 CCD camera. For treatment, 5-d-old seedlings of *ABP1$_{i1,2}$::GUS* were transferred to ½ MS media supplemented with DMSO (mock) for 3.5 h, 25 μM L-Kynurenine (Sigma-Aldrich, 2922-83-0) for 3.5 h and 25 μM L-Kynurenine for 2 h followed by 300 nM IAA (Duchefa, 87-51-4) for 1.5 h. Subsequently, GUS staining and DIC microscopy were performed as described above.

2.5. Quantitative real-time PCR

After treatment with 100 nM IAA, seedlings were sampled in 4 biological replicates at different times (t0, 5 min, 30 min, 1 h, 2 h and 4 h). Total RNA was prepared from max100 mg of shoots/roots of 5-d-old seedlings with the RNeasy Plant Mini Kit (Qiagen, 74904) according to the manufacturers's instructions. cDNA was synthesized from 2 μg of total RNA using the QuantiNova Reverse Transcription Kit (Qiagen, 205410). For the mutant expression analyses, 3 biological replicates of full seedlings were used. All samples were pipetted in 3 technical replicates in a 384 well plate using an automated JANUS Workstation (PerkinElmer). According to the manufacturer's instructions, 5 μL reaction volume contained 2.5 μL Luna® Universal qPCR mastermix (NEB, M3003S). RT-qPCR analyses were performed using the Real-time PCR Roche Lightcycler 480 and the expression of PP2AA3 (At1G13320) or EF1a (At5G60390) was used as a reference [47]. For *ABP1*, 5 different primer pairs were evaluated and one representative graph is included in the manuscript. The primers used for the presented analysis are listed in Supplemental Table 2.

2.6. Confocal laser scanning microscopy and image analysis

Confocal laser scanning microscopy for analysis of fluorescence intensity was performed on a Zeiss LSM800 microscope assisted with Zeiss Zen 2011 software. Images were acquired with 20x/0.8 NA air (DR5 evaluation) or 40x/1.2 NA water immersion objectives (immunostaining).

2.7. DR5-GFP intensity measurement

5-d-old seedlings were transferred from solid ½ MS media to plates supplemented with either DMSO or 1 μM IAA for 3 h and imaged using confocal microscopy. The fluorescence intensity of GFP (excitation wavelength: 488 nm) was measured in ImageJ.

2.8. Microfluidic vRootchip

A microfluidic chip, vRootchip was used to analyze root tip growth in real-time. The manufacturing of the chip, sample preparation procedure, and data analysis of root tip growth was performed as described previously [16] and according to Li and Verstraeten *et al.* (unpublished). vRoot-chip was used with 10 nM IAA treatment in ¼ MS and 0.1 % sucrose. For imaging, the vertical confocal microscopy setup was used as described previously [16,48] and according to Li and Verstraeten et al. (unpublished). The 10 nM IAA solution was supplemented with the cell-impermeable fluorescent dye Tetramethylrhodamine iso-thiocyanate–Dextran [16].

2.9. Protoplast assay

Protoplasts from 3-d-old Arabidopsis root suspension culture were isolated and transformed as previously described [49]. Plasmids were prepared with an E.Z.N.A. Plasmid Maxi Kit I (Omega Bio-Tek, D6922-02). Protoplasts were co-transfected with 6 μg of *35S::ABP1* or *35S::ABP1-M2X*, 2.5 μg of *DR5::LUC* [50] and 2.5 μg of *35S::Renilla* [51]. As a control, protoplasts co-transfected with *DR5::LUC* and *35S::Renilla* were used. The protoplasts were incubated with either 100 nM NAA (Sigma-Aldrich, 86-87-3) for 16 h or without treatment for 12 h followed by 100 nM NAA for 4 h in the dark at room temperature. The corresponding amount of DMSO was used as mock treatment. Chemiluminescence measurement was performed with the Dual-Luciferase Reporter Assay System kit (Promega, E1910) using a Spectrophotometer BioTek SynergyH1 plate reader and Gen 5 software (both BioTek).

2.10. Root length analysis

Plates with 4- and 7-d-old seedlings were scanned using an Epson Perfection V370 Photo flatbed scanner and the root length was measured using ImageJ.

2.11. Root gravitropic assay

For measurements of root gravitropic curvature kinetics, 4-d-old seedlings were placed on plates with ½ MS and rotated 90° and roots were imaged using a vertically placed flatbed scanner (Epson Perfection V370 Photo). Multiple plates were held in place on the scanner by a custom-made holder. Max. 12 ROIs of the seedlings were automatically imaged with a resolution of 1200 dpi in 10 min time intervals using an AutoIt script for 8 h. In ImageJ, the time-lapse movies of the seedlings were manually cropped and registered (stabilized) using the Fiji plugin "StackReg" in "Rigid body" mode.

2.12. Root growth (RG)-tracker

We developed a custom MATLAB application named RG-tracker (https://research-explorer.app.ist.ac.at/librecat/record/8294) with a graphical user interface that allows entirely automated root growth analysis and tracking of the root tips. Root tips were segmented based on the pixel classification workflow of Ilastik [52], which only requires manual retraining in case the imaging conditions change drastically. For each point in time, the positions of the root tips were determined by segmenting the tip-probability output, performing particle size filtering and calculating the center of mass. The root tips were then tracked over time by solving the linear assignment problem using the Hungarian

algorithm (Munkres). The tracking algorithm can deal with gaps in the root tip detection and both the gap closing and the maximum linking distance can be specified in the GUI. Completed tracks are filtered by minimum track length, duration and maximum growth speed to remove miss-detections and then presented to the user as an overlay of raw data, tip segmentation and tip tracks. At this point the user can exclude additional tracks from further analysis and export the overlay of the tracks and the root time-lapse. The x/y coordinates of each root tip, growth speed, direction of growth, growth angle and root length are then calculated for each point in time and exported for further analysis. All experiment specific parameters such as the segmentation threshold, particle size, and track filters can be saved and together with the segmentation project file form the complete data set to clearly recapitulate the data analysis.

2.13. Lateral root analysis

For the analysis of lateral root primordia, samples of 6-d-old seedling were collected and the tissue was cleared as previously described [46]. To visualize the lateral root primordia DIC microscopy was performed using an Olympus BX53 microscope equipped with a 20x air objective. The lateral root primordia were staged according to Malam and Benfey (1997) [46]. For analysis of emerged lateral roots, 4-d-old seedlings were transferred from ½ MS plates to plates supplemented with 500 nM NAA or DMSO. After 3 days, the plates were scanned using an Epson Perfection V370 Photo flatbed scanner and the pictures were analyzed using ImageJ.

2.14. Etiolated hypocotyl growth

To analyze the growth of etiolated hypocotyls, the seedlings were recorded at 12 h intervals for 120 h in a dark chamber equipped with an infrared light source (880 nm LED; Velleman, Belgium) and a spectrum-enhanced camera (EOS035 Canon Rebel Xti, 400DH) with built-in clear wideband-multicoated filter and standard accessories (Canon) and operated by the EOS utility software. The hypocotyl length was measured using ImageJ.

2.15. Etiolated hypocotyl bending

To determine hypocotyl gravitropism, the 3-d-old dark grown seedlings were rotated 90°. The plates were scanned using an Epson Perfection V370 Photo flatbed scanner and the hypocotyl bending angle was measured after gravity stimulation in 6 h intervals for 24 h using ImageJ.

2.16. Rosette size analysis

Seeds were germinated and grown on horizontally placed plates for 12 days, scanned using an Epson Perfection V370 Photo flatbed scanner and the rosette size was measured manually in ImageJ.

2.17. Vasculature development analysis

10-d-old cotyledons were collected and the tissue was cleared as follows: 2 days incubation in 70 % ethanol with a subsequent incubation in 4 % HCl, 20 % methanol solution at 65 °C for maximum 15 min, followed by an incubation in 7 % NaOH, 60 % ethanol solution at RT for another 15 min. The cotyledons were then re-hydrated in a series of decreasing ethanol concentrations (60 %, 40 %, 20 % and 10 %) for 1 h in each concentration at RT. Before mounting the cotyledons in 50 % glycerol onto microscopy slides they were incubated for 1 h in 25 % glycerol, 5 % ethanol solution at RT. Imaging was done using an Olympus BX53 microscope equipped with a 4x air objective.

2.18. Hypocotyl growth under high temperature

Seeds were germinated and grown on ½ MS plates with or without 10 g/L sucrose under 28 °C, continuous light for 7 days. The plates were scanned using an Epson Perfection V370 Photo flatbed scanner and the hypocotyl length was measured using ImageJ.

2.19. Hyperosmotic stress assay

4-d-old seedlings were transferred on media supplemented with either 200 mM mannitol or 100 mM NaCl for 4 days. The plates were scanned using an Epson Perfection V370 Photo flatbed scanner and the root extension was measured using ImageJ.

2.20. UV laser ablation and periclinal division analysis

3-d-old seedlings were transferred from solid ½ MS medium to plates containing 10 μM propidium iodide (Sigma-Aldrich, 25535-16-4) supplemented with 1 μM NAA or DMSO. The subsequent sample preparation, UV laser ablation, imaging and periclinal cell division analysis was performed as described previously [53].

2.21. Bolting time, leaf number and branch number analysis

Seeds were suspended in 0.1 % agarose and spread out in soil. The number of plants, bolted and with the primary inflorescence stem grown 1 cm, was recorded every day. The number of rosette and cauline leaves was counted when the first flower of each plant bloomed. The rosette branch was referred to the branch directly attached to the rosette, while the cauline branch was defined as the branch on the primary stem. The number of cauline branches and rosette branches were counted 21 days after sowing.

2.22. Phyllotaxis and internode length measurement

Analyses of 25 plants per genotype were performed when the last flowers had appeared. Angles and internode lengths between two subsequent siliques were measured starting from the lowest one. For each individual of each genotype, the variance of the divergence angles was computed, and individual variances of divergence angles were compared between genotypes using a non-parametric Kruskal–Wallis test in R (version 3.5.1, r-project.org), since their values were not normally distributed.

2.23. Immunostaining

Immunostaining was performed with 3 to 4-d–old seedlings as previously described [54]. The primary antibodies used were rabbit anti-PIN1 [9] diluted 1:1000 (v/v) and rabbit anti-PIN2 [55] diluted 1:1000 (v/v). The secondary antibody used was sheep anti-rabbit conjugated with Cy3 (Sigma-Aldrich, C2306) diluted 1:600 (v/v).

2.24. PIN lateralization

3to 4-d-old seedlings were treated either with 10 μM NAA or DMSO as a control for 4 h in liquid ½ MS medium. Subsequently, immunostaining using PIN1 and PIN2 antibodies was performed. Samples were imaged using confocal microscopy. The fluorescence intensity of Cy3 (excitation wavelength: 548 nm) was measured using ImageJ.

2.25. BFA treatment

4-d–old seedlings were incubated in liquid ½ MS medium at a final concentration of 25 μM BFA (Sigma-Aldrich, 20350-15-6) for 1 h. For BFA/NAA treatment the seedlings were pre-treated with 5 μM NAA for 30 min followed by co-treatment with 25 μM BFA and 5 μM NAA for 1 h.

As control, seedlings were incubated in liquid ½ MS medium supplemented with DMSO substituting NAA. Subsequently, immunostaining using PIN1 and PIN2 antibodies was performed. Samples were imaged using confocal microscopy and the fluorescence signal of Cy3 (excitation wavelength: 548 nm) was detected. BFA body formation was scored from 0 (no BFA body formation) to 3 (maximal BFA body formation) for each image, reflecting both the number of cells with BFA bodies as well as size and number of BFA bodies per cell. To avoid cognitive bias, all images were encoded prior to analysis.

2.26. Global transcriptome data analysis

Tissue-specific expression pattern and expression following different perturbations were obtained using Genevestigator (www.genevestigator.com) and were based on the 'AT_AFFY_ATH1-0' dataset.

2.27. Statistical analysis

If not mentioned differently, all data were analyzed using Student's t tests with p-value (*, $P < 0.05$; ** $P < 0.01$; *** $P < 0.001$) in the software Prism v8.3.0 (GraphPad).

2.28. Accession numbers

Sequences data from this article can be found in the GenBank/EMBL libraries under the following accession numbers: ABP1 (AT4G02980); PP2AA3 (At1G13320); EF1a (At5G60390).

3. Results

3.1. ABP1 expression and regulation by auxin

To obtain indications regarding the developmental processes and conditions in which ABP1 might play a role, we analyzed the *ABP1* expression pattern. The analysis of publicly available global transcriptome data in GENEVESTIGATOR® [56] suggested that *ABP1* is expressed constitutively in different tissues during development. *ABP1* transcription appears to be the highest in rosette leaves and roots, whilst lowest in pollen (Fig. S1A-B). In seedlings, *ABP1* is expressed in cotyledons, hypocotyls and root tips as well as in lateral roots. Global transcriptomics data following different perturbations suggested that *ABP1* expression is elevated in response to heat and slightly decreased following biotic stress (Fig. S1C).

To obtain more detailed insight into the *ABP1* expression pattern and confirm the global transcriptome analysis-based notions, we used an *ABP1::GUS* line to report *ABP1* promoter activity *in vivo*. GUS staining of
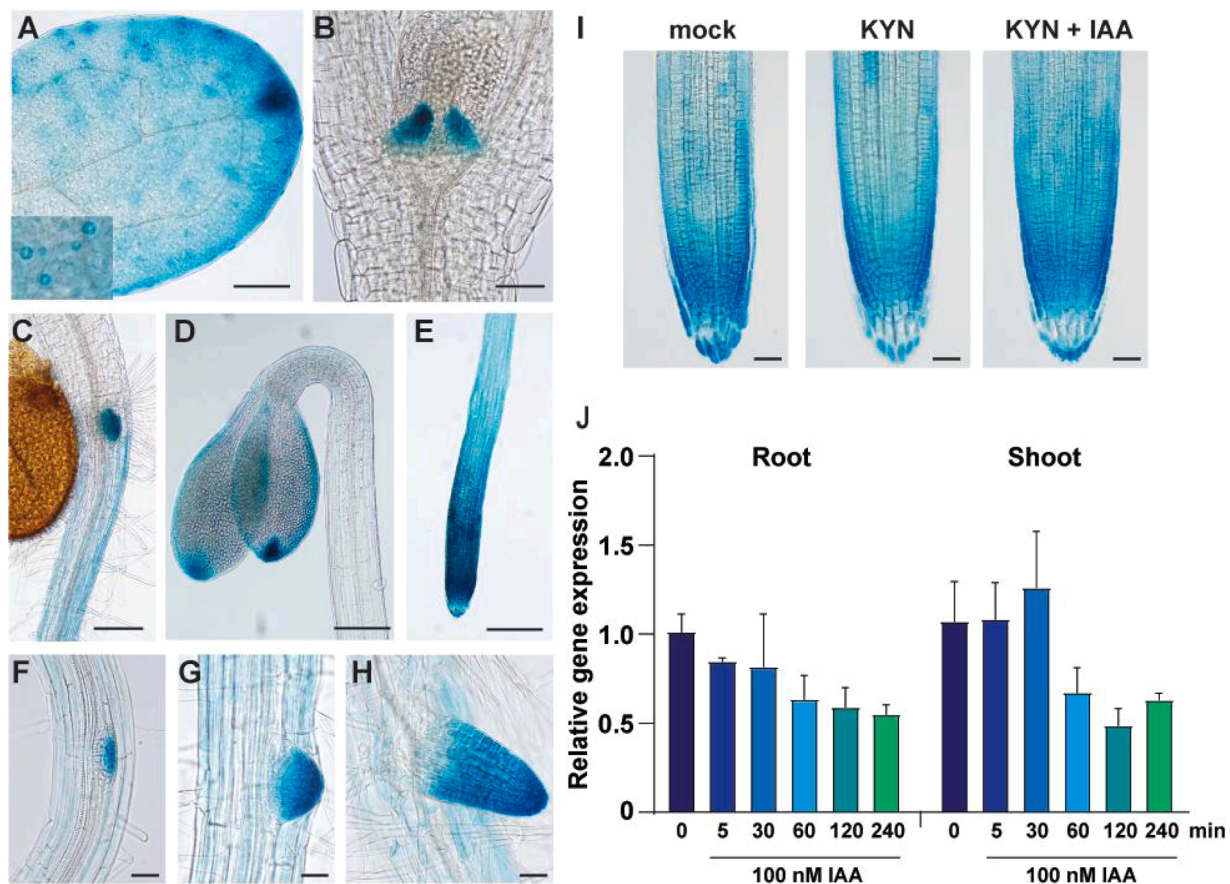

Fig. 1. *ABP1* expression and regulation by auxin.

(A–H) *ABP1::GUS* expression pattern. (A) 6-d-old cotyledon with inset detail of stomata, scale bar =100 μm. (B) shoot with hydathods of 6-d-old seedling, scale bar =50 μm. (C) shoot-root junction of 6-d-old seedling, scale bar =50 μm. (D) apical hook of 3-d-old etiolated seedling, scale bar =100 μm. (E) root tip of 6-d-old seedling, scale bar =100 μm. (F–H) lateral root primordia of 6-d-old seedling in IV, V and emerged stage respectively, scale bar =20 μm.

(I) Representative pictures of *ABP1::GUS* expression pattern in 5-d-old seedlings after treatment with DMSO (mock) for 3.5 h, 25 μM L-Kynurenine for 3.5 h and 25 μM L-Kynurenine for 2 h followed by 300 nM IAA for 1.5 h. For each treatment, at least 15 seedlings were evaluated. The experiment was repeated 2 times with similar results. Scale bar =20 μm.

(J) Quantitative Real-time PCR of *ABP1* expression in roots and shoots of 5-d-old Col-0 seedlings after DMSO (mock), and 5 min, 60 min, 120 min and 240 min of 100 nM IAA treatments. Expression of *ABP1* is normalized on expression of *PP2A* housekeeping gene. Experiment was repeated 3 times with similar result.

6-d-old seedlings confirmed the *ABP1* expression in cotyledons in which we detected stronger *ABP1* promoter activity in hydathodes and stomata (Fig. 1A-B). In both light- and dark-grown hypocotyls, the *ABP1* promoter activity was very low (Fig. 1C–D). Further, we confirmed *ABP1* expression in the primary root, particularly in the root tip (Fig. 1E) and during different stages of lateral root development (Fig. 1F–H). We observed that *ABP1* expression pattern in hydathodes, root tip and lateral roots largely overlaps with that of *DR5* reporters for transcriptional auxin response [43,44,50,57–59].

Therefore, we tested whether auxin regulates *ABP1* promoter activity and transcription. We employed L-Kynurenine, an inhibitor of auxin biosynthesis [60], to decrease auxin levels in the *ABP1::GUS* seedlings.

We tested both, the effect of L-Kynurenine treatment alone or with subsequent auxin treatment, to study the effect of exogenously applied auxin. Overall, we detected no obvious changes in GUS reporter activity either after L-Kynurenine or after L-Kynurenine followed by auxin treatments (Fig. 1I).

To additionally verify these observations, we examined the auxin effect on *ABP1* transcription using real-time quantitative PCR (RT-qPCR). We performed RT-qPCR with roots and shoots of 5-d-old wild-type seedlings after auxin treatment. Consistent to what we observed with the *ABP1::GUS* transgenic line, auxin treatment did not strongly affect *ABP1* transcription (Fig. 1J).

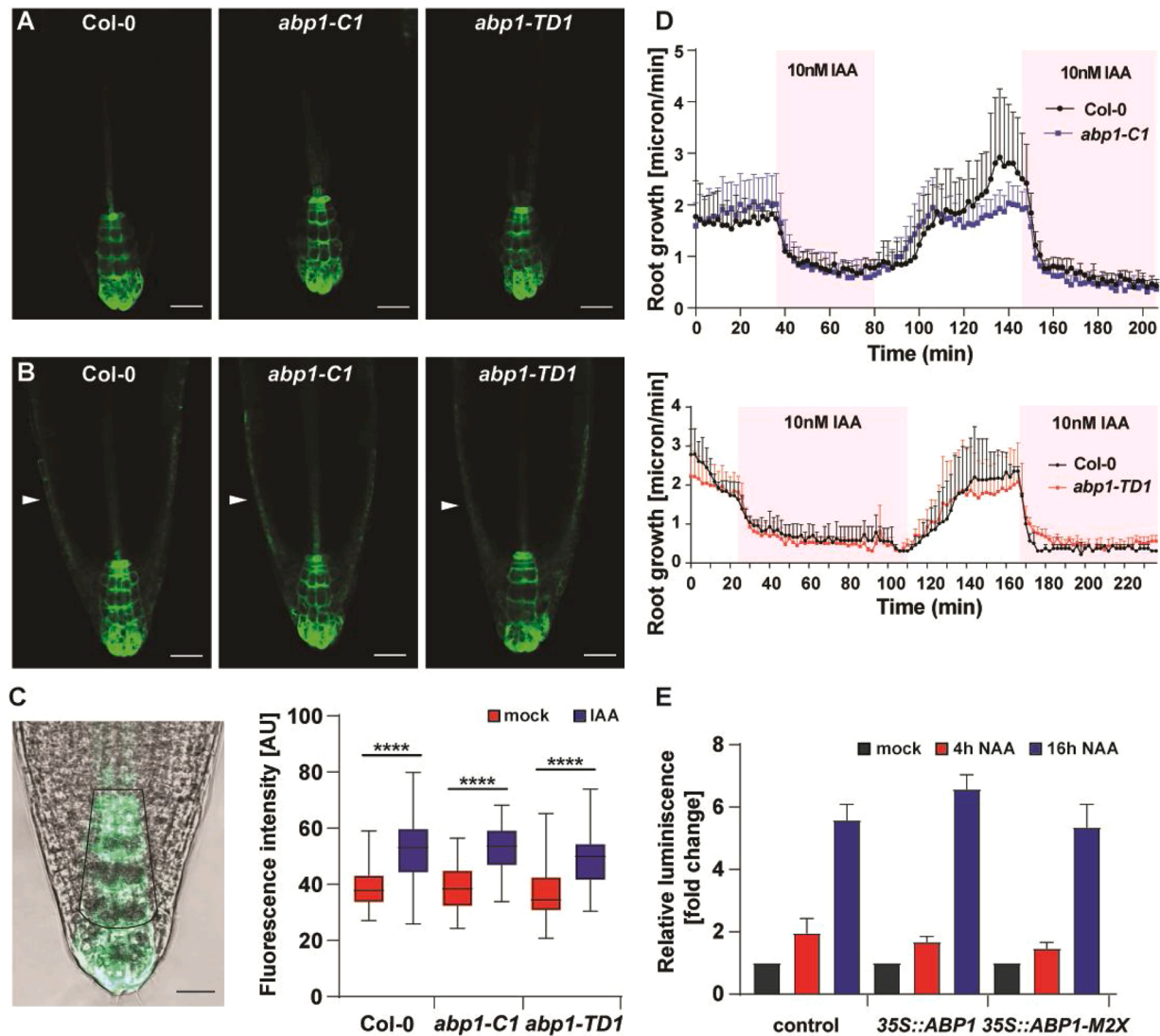These results show that *ABP1* expression overlaps with auxin

Fig. 2. Involvement of ABP1 in TIR1/AFB-mediated auxin responses.
(A–B) *DR5rev::GFP* expression pattern in 5-d-old seedlings of wild-type Col-0, *abp1-C1* and *abp1-TD1* mutants with DMSO (A) or with 1 μM IAA (B) treatment for 3 h. Arrowheads point to DR5 signal expanded to lateral root cap. Scale bar =30 μm.
(C) Representative picture of *DR5rev::GFP* expression in Col-0 with highlighted region that was quantified. Scale bar =50 μm. Quantification of *DR5rev::GFP* signal in root tips of 5-d-old Col-0, *abp1-C1* and *abp1-TD1* seedlings with DMSO (A) or with 1 μM IAA (B) treatment for 3 h. For each genotype per treatment, at least 15 seedlings were measured. The pooled result of 2 independent experiments is presented. For box plot, box defines the first and third quartiles, and the central lines in the box represent the median. Whiskers, from minimum to maximum. Asterisks indicate significant differences according to Student's t-tests (****, P < 0.0001).
(D) Root growth rate of *abp1-C1* (upper graph) and *abp1-TD1* (lower graph) compared to Col-0 measured in the vRootchip with repetitive 10 nM IAA treatment (magenta). n = 5, 6 for Col-0 and *abp1-C1*, respectively. n = 5 for *abp1-TD1*; n = 3,2 for Col-0 from 0−102 min and 102−236 min, respectively. Error bars denote standard deviation. The experiment was repeated 2 times with similar results.
(E) Activity of *DR5::LUC* reporter in response to *ABP1* and *ABP1-M2X* overexpression after mock (DMSO) and 100 nM IAA treatment in protoplasts. The values presented were calculated as a ratio between *DR5::LUC* enzymatic activity and internal control *Renilla::LUC* enzymatic activity and were further normalized on mock treatment values. Error bars denote standard error. The statistical difference was tested by Student's t-test. The experiment was repeated 2 times with similar results.

response maxima during seedling development, but that *ABP1* promoter activity and *ABP1* transcription are not significantly regulated by auxin.

3.2. Involvement of ABP1 in TIR1/AFB-mediated auxin responses

Considering that *ABP1::GUS* expression pattern largely overlaps with that of DR5 reporters for transcriptional auxin response [43,44,50, 57–59], we investigated whether *ABP1* function is in any way linked to the transcriptional auxin signaling downstream of TIR1/AFB receptors [12,61]. First, we introduced *DR5rev::GFP* reporter into *abp1* loss-of-function mutants (*abp1-C1* and *abp1-TD1*). In the *abp1* mutant backgrounds, *DR5rev::GFP* expression pattern in the root tip was not visibly altered and showed the typical maximum in the columella cells and quiescent center [57,58,62] (Fig. 2A). After auxin treatment, the *DR5rev::GFP* signals in *abp1* mutants expanded to the lateral root cap and stele to the same extent as in the control (Fig. 2B). Quantification of the DR5 signal without and with auxin treatment in the root tips did not reveal any differences between the control and *abp1* mutants (Fig. 2C). Taken together, these results show that the DR5 auxin response reporter's readout does not depend on a functional *ABP1*.

Recently it was demonstrated, that the TIR1/AFB pathway is required for a rapid non-transcriptional auxin response [16]. We used this experimental system to investigate TIR1/AFB-mediated non-transcriptional auxin effects on root growth in the mutant lines. Evaluation of root growth on the vertical imaging set-up with high spatio-temporal resolution [16,48] revealed a comparable auxin sensitivity of the *abp1-C1* and *abp1-TD1* mutants and the control line in terms

of rapid inhibition of root growth (Fig. 2D) suggesting that *abp1* loss-of-function does not affect the TIR1/AFB-mediated non-transcriptional response.

Next, we tested the effect of *ABP1* gain-of-function on TIR1/AFB-mediated transcriptional auxin signaling by performing a transient expression assay in Arabidopsis protoplasts. We derived protoplasts from root cell culture, co-transfected them with *DR5::LUC* reporter together with either *35S::ABP1* or *35S::ABP1-M2X* carrying a mutation in the auxin-binding site [35] and measured the *DR5::LUC* signal with and without auxin. The DR5-driven luciferase activity increased after both short (4 h) and long (16 h) term auxin treatment, however neither *ABP1* nor *ABP1-M2X* overexpression had any significant influence on this induction (Fig. 2E).

These results do not support a strict requirement of *ABP1* function in the canonical, TIR1/AFB-mediated auxin signaling pathway.

3.3. Role of ABP1 in primary root growth and root gravity response

Since *ABP1* is expressed in the primary root and root tip (Fig. 1C, E) and auxin is a major regulator of root growth [16,63–65], we analyzed whether *abp1* loss-of-function or the overexpression influences primary root growth. We used two independent loss-of function mutant lines, *abp1-C1* and *abp1-TD1* and a line expressing *ABP1-GFP* under the control of the ubiquitous 35S promoter (*ABP1-GFP*[OE]) (Fig. S2). Visually, roots of all tested lines developed normally (Fig. 3A). We measured the root length of 4- and 7-d-old seedlings and found that the root growth of *abp1* mutants was comparable to WT, while roots of *ABP1-GFP*[OE] were shorter
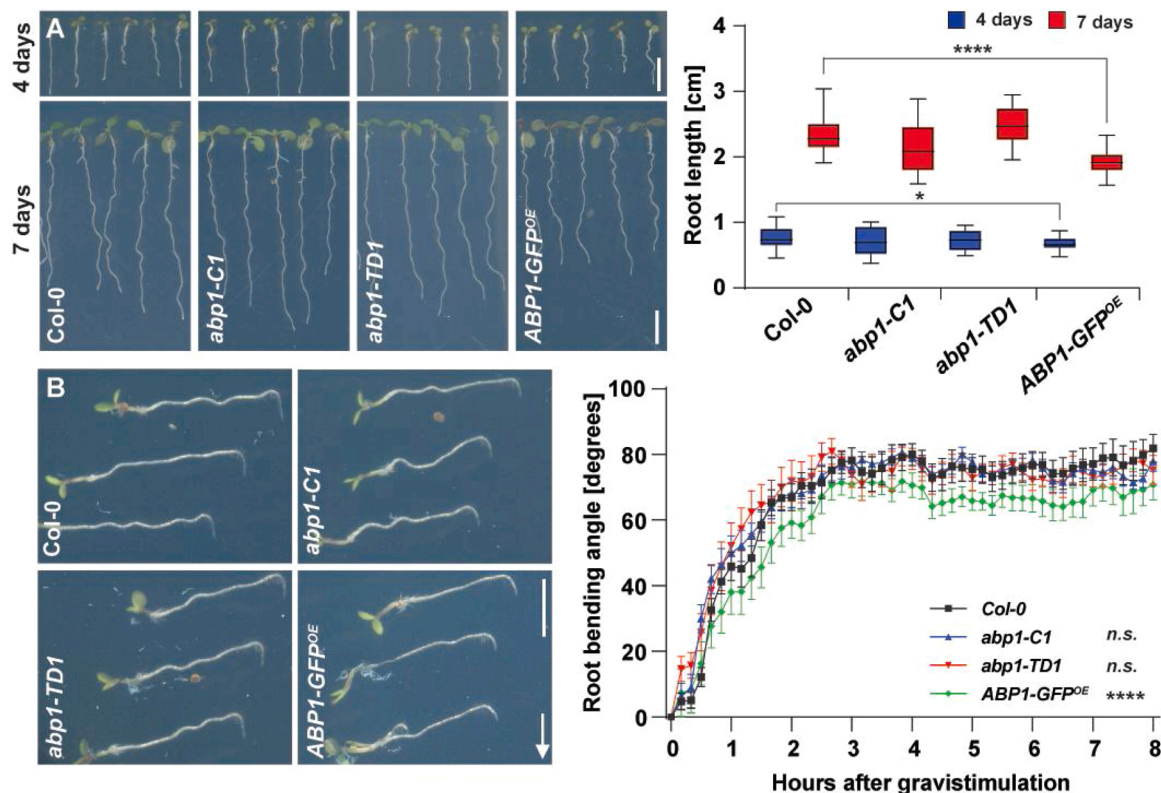

Fig. 3. Role of ABP1 in primary root growth and root gravity response.
(A) Representative images of 4- (upper panel) and 7-d-old (lower panel) Col-0, *abp1-C1*, *abp1-TD1*, and *ABP1-GFP*[OE] seedlings. Scale bar =5 mm. The boxplot shows the root length of 4- and 7-d-old Col-0, *abp1-C1*, *abp1-TD1*, and *ABP1-GFP*[OE] seedlings. For each genotype, at least 15 roots were measured. For box plot, box defines the first and third quartiles, and the central lines in the box represent the median. Whiskers, from minimum to maximum. Asterisks indicate significant differences according to Student's t tests (*, P < 0. 05; ****, P < 0. 0001). The experiment was repeated 2 times with similar results.
(B) Representative images of 4-d-old Col-0, *abp1-C1*, *abp1-TD1*, and *ABP1-GFP*[OE] seedlings after 8 h gravistimulation by 90° reorientation. Scale bar =1 cm. Arrow indicates gravity direction. Kinetics of root bending during 8 h of gravity stimulus for Col-0, *abp1-C1*, *abp1-TD1*, and *ABP1-GFP*[OE]. For each line at least 15 roots were measured. Error bars denote standard deviation. Asterisks indicate significant differences according to Student's t tests (****, P < 0. 0001). The experiment was repeated 2 times with similar results.

(Fig. 3A).

Asymmetric auxin distribution is involved in gravitropism, an important plant adaptive process manifested by shoot and root bending [66–69]. In order to describe a role of *ABP1* during root bending, we gravistimulated (90° reorientation) roots of 4-d-old *abp1* and *ABP1-GFP^{OE}* seedlings for 8 h and measured the root bending kinetics. We observed that *abp1* mutants showed a normal root gravitropic response while the roots of *ABP1-GFP^{OE}* bent significantly slower (Fig. 3B).

In summary, the *abp1* loss-of-function mutants do not have any impact on either root growth or root bending, whereas gain-of-function leads to slower root growth and root bending.

3.4. Role of ABP1 during lateral root development

As *ABP1* is expressed during lateral root development (Fig. 1F–H), and auxin promotes lateral root initiation and formation [59], we analyzed lateral root development in 6-d-old *abp1* and *ABP1-GFP^{OE}*

seedlings. We counted and scored all lateral root primordia stages. The analysis revealed that both *abp1* mutants and *ABP1-GFP^{OE}* developed a comparable number of lateral root primordia (Fig. 4A). In addition, we could not find any differences in the frequency of individual primordial stages (Fig. 4B).

To test the auxin effect on lateral root emergence, we transferred 4-d-old seedlings to media supplemented with auxin and 3 days later we counted the density of emerged lateral roots. We observed that the density of emerged lateral roots was comparable between *abp1* mutants and WT, while *ABP1-GFP^{OE}* developed less lateral roots (Fig. 4C).

Together, the results presented above demonstrate that both *abp1* loss-of-function mutants do not have any impact on lateral root development, but that *ABP1* overexpression leads to impaired auxin-induced lateral root development.

3.5. Role of ABP1 in etiolated growth and shoot gravity response

Auxin is required for a sustained rapid hypocotyl-elongation of
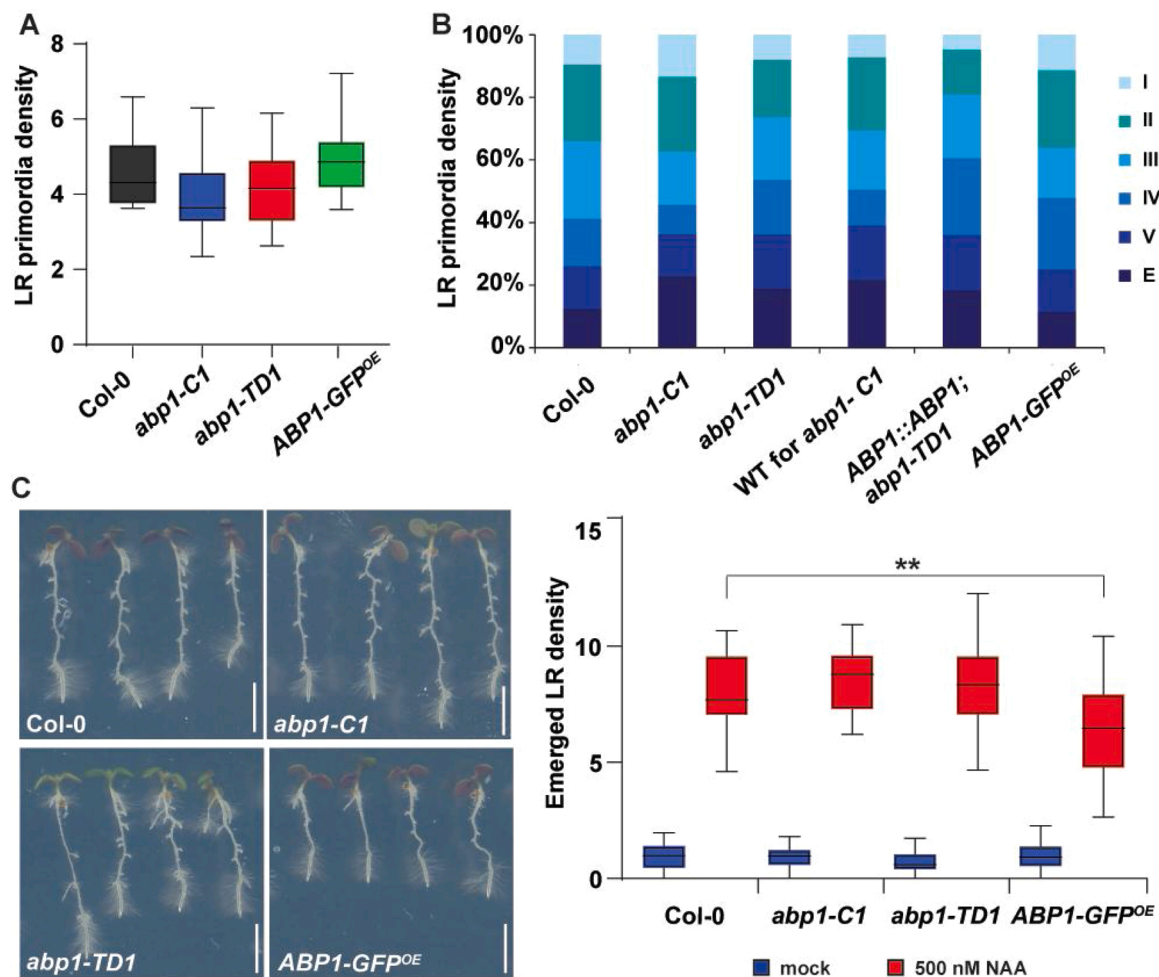

Fig. 4. Role of ABP1 during lateral root development.
(A) Density of lateral root (LR) primordia in 6-d-old Col-0, *abp1-C1*, *abp1-TD1*, and *ABP1-GFP^{OE}* seedlings. For each line, primordia of at least 15 roots were counted. For box plot, box defines the first and third quartiles, and the central lines in the box represent the median. Whiskers, from minimum to maximum. The statistical difference was tested by Student's t-test. The experiment was repeated 2 times with similar results.
(B) Density of individual lateral root primordia stages in 6-d-old Col-0, *abp1-C1*, *abp1-TD1*, WT for *abp1-C1* as control for *abp1-C1*, complemented *abp1-TD1* mutant (*ABP1::ABP1;abp1-TD1*) as control for *abp1-TD1*, and *ABP1-GFP^{OE}* seedlings expressed as percentage. For each line, primordia of at least 15 roots were scored. The experiment was repeated 2 times with the similar results.
(C) Representative pictures of Col-0, *abp1-C1*, *abp1-TD1*, and *ABP1-GFP^{OE}* roots 3 days after 500 nM NAA treatment. Scale bar =5 mm. The box plot shows emerged lateral root density. For each line at least 15 roots were scored. For box plot, box defines the first and third quartiles, and the central lines in the box represent the median. Whiskers, from minimum to maximum. Asterisks indicate significant differences according to Student's t tests (** $P < 0.01$). The experiment was repeated 2 times with similar results.

plants grown in darkness [70–72]. The auxin-induced growth of etiolated hypocotyl segments is not altered in *abp1* loss-of-function mutants [15]. To complement these observations in intact plants, we analyzed growth of etiolated hypocotyls for both *abp1* loss- and gain-of-function lines and measured the hypocotyl length of the dark-grown seedlings every twelve hours (Fig. 5A). Initially, the hypocotyls of all tested lines elongated at the same speed. Later, starting 36 h after germination, etiolated hypocotyls of *ABP1-GFP^OE* elongated faster and they were significantly longer than the control 120 h after germination. On the other hand, etiolated hypocotyls of both *abp1* mutant alleles elongated comparably to the controls.

The gravitropic response of the hypocotyl is also regulated by auxin [67–69]. To investigate a possible function of *ABP1* in hypocotyl gravitropism, we gravistimulated 3-d-old etiolated hypocotyls and measured the bending angle after 6, 18 and 24 h. The analysis revealed that the *ABP1-GFP^OE* hypocotyls bend significantly less than WT (Fig. 5B). The difference was noticeable already 6 h after gravistimulation. Notably, both *abp1* mutants showed a similar tendency towards slower bending, albeit not significant.

In summary, these observations unveiled that *abp1* loss-of-function alleles do not show defects in etiolated hypocotyl growth and gravitropic responses, whereas gain-of-function of *ABP1* leads to increased elongation and defective gravity-mediated hypocotyl bending.

3.6. Role of ABP1 in leaf development and vasculature formation

In cotyledons, auxin and its directional transport act as a positional cue for vasculature vein formation [73,74] and also regulate leave shape and serration [75]. We analyzed whether ABP1 plays a role in the young rosette growth and development as well as in cotyledon vasculature formation. Macroscopically, neither *abp1* mutants nor *ABP1-GFP^OE* showed any defects in cotyledon development (Fig. 6A). We measured the size of young rosettes consisting of both cotyledons and primary leaves. We found that *ABP1-GFP^OE* had slightly bigger rosettes (Fig. 6A).

The vasculature of cotyledons typically consists of four formed closed loops (Fig. 6B). We scored the number and the completeness of these loops in *abp1* mutants and *ABP1-GFP^OE*. We observed a normal vasculature pattern in both *abp1* mutants, but *ABP1-GFP^OE* showed irregularities at higher frequency than WT (Fig. 6B). The most striking difference in *ABP1-GFP^OE* were fewer loops (22 % in WT and 46 % in *ABP1-GFP^OE*) and loops that were opened at their upper end, which is almost never seen in WT (2 % in WT and 6.5 % in *ABP1-GFP^OE*).

The results show that, whilts *abp1* loss-of-function has no impact on leaves growth and venation, *ABP1* gain-of-function affects vasculature formation.

3.7. Role of ABP1 during stress

Abiotic stresses, such as salinity and osmotic stress, induce changes in turgor pressure and in polar auxin transport [76–78] and thus lead to root growth inhibition. On the other hand, an increase of auxin biosynthesis results in higher salt tolerance [79,80]. The regulation of *ABP1* transcription by various stresses such as heat (Fig. S1) prompted us to test the requirement of *ABP1* to adapt to stress.

We challenged *abp1* mutants with osmotic stress using mannitol or sodium chloride treatments to assess the involvement of *ABP1* in stress
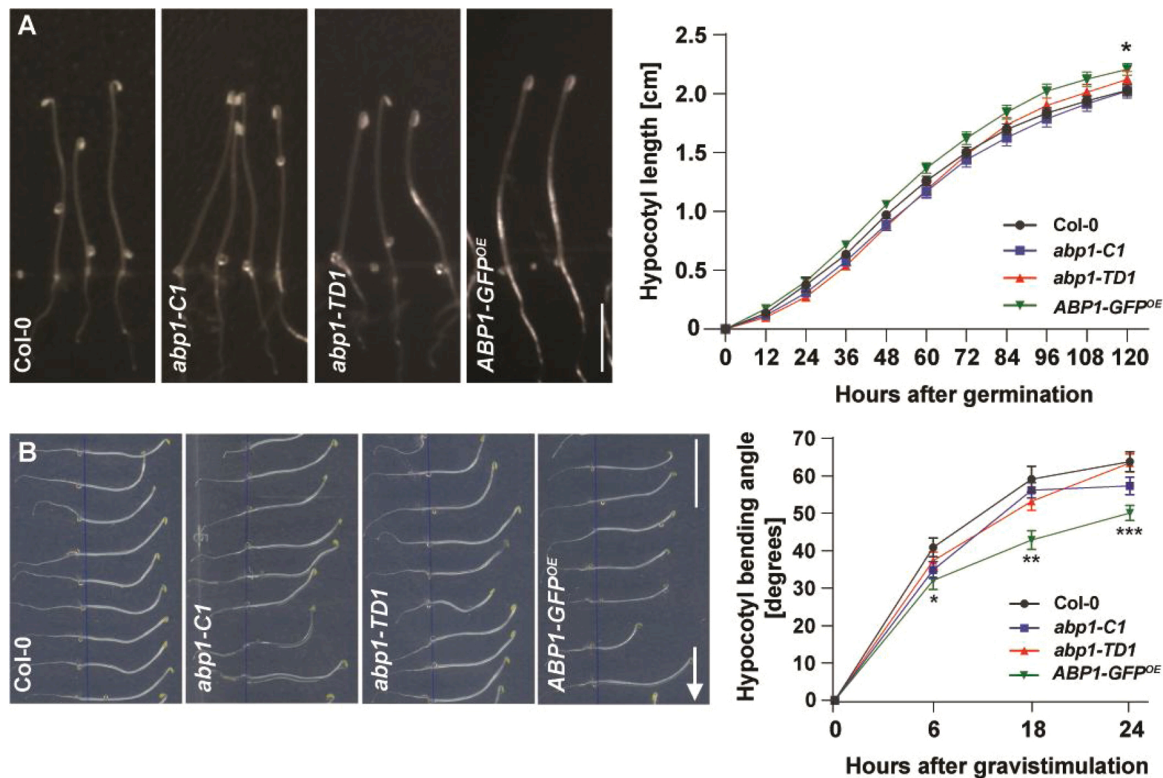

Fig. 5. Role of ABP1 in etiolated growth and shoot gravity response.
(A) Representative images of 3-d-old etiolated hypocotyls of Col-0, *abp1-C1*, *abp1-TD1*, and *ABP1-GFP^OE*. Scale bar =1 cm. Elongation rate of Col-0, *abp1-C1*, *abp1-TD1*, and *ABP1-GFP^OE* etiolated hypocotyls. For each line at least 10 hypocotyls were measured. Error bars denote standard error. The experiment was repeated for 2 times with similar results. Asterisks indicate significant differences according to Student's t tests (*, P < 0. 05).
(B) Representative images of 24 h gravity stimulated etiolated hypocotyls of Col-0, *abp1-C1*, *abp1-TD1*, and *ABP1-GFP^OE*. Scale bar =1 cm. Arrow indicates gravity direction. Kinetics of hypocotyl bending of Col-0, *abp1-C1*, *abp1-TD1* and *ABP1-GFP^OE* during 24 h of gravity stimulation. For each line at least 10 hypocotyls were measured. Error bars denote standard error. Asterisks indicate significant differences according to Student's t tests (*, P < 0. 05; ** P < 0. 01; *** P < 0. 001). The experiment was repeated 3 times with similar results.
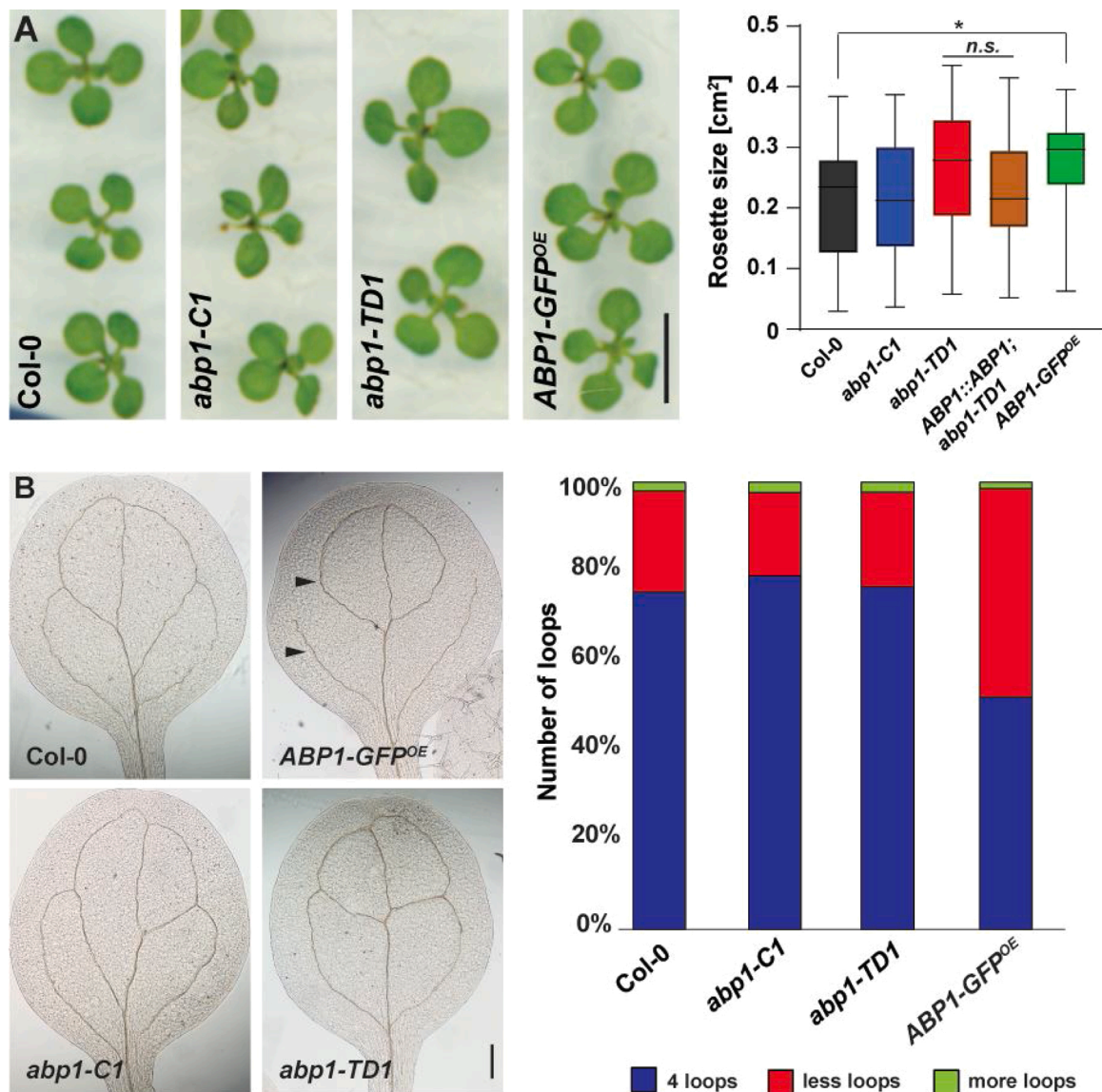
Fig. 6. Role of ABP1 in leaf development and vasculature formation.

(A) Representative images of the rosettes of 12-d-old of Col-0, *abp1-C1*, *abp1-TD1* and *ABP1-GFP*^{OE} seedlings. Scale bar =5 mm. The boxplot shows the size of the rosettes for Col-0, *abp1-C1*, *abp1-TD1*, complemented *abp1-TD1* mutant (*ABP1::ABP1;abp1-TD1*) as control for *abp1-TD1*, and *ABP1-GFP*^{OE}. For each genotype and experiment, more than 19 rosettes from 12-d-old seedlings were measured. For box plot, box defines the first and third quartiles, and the central lines in the box represent the median. Whiskers, from minimum to maximum. Asterisks indicate significant differences according to Student's *t*-tests (*, P < 0.05). The experiment was repeated 2 times with the similar result.

(B) Representative pictures of cotyledons venation pattern of 10-d-old Col-0, *abp1-C1*, *abp1-TD1* and *ABP1-GFP*^{OE} seedlings. Scale bar =200 μm. Arrowheads point to typical vasculature defects in *ABP1-GFP*^{OE}. Quantification of number of loops in 10-d-old cotyledons of Col-0, *abp1-C1*, *abp1-TD1* and *ABP1-GFP*^{OE} is presented as percentage. For each line at least 20 cotyledon leaves were scored. The experiment was repeated 2 times with similar results.

responses. Overall, following the treatments, root growth and lateral root formation of WT and *abp1* mutants were inhibited (Fig. 7A–C). In addition, no obvious differences in root growth inhibition were observed after mannitol or sodium chloride treatment between the tested lines (Fig. 7B–C).

High temperature promotes auxin biosynthesis, thereby leading to rapid hypocotyl growth [70]. To address a potential role of *ABP1* in auxin-mediated rapid hypocotyl growth in response to high temperature and the presence of sugar, we characterized hypocotyl elongation of *abp1* and *ABP1-GFP*^{OE} seedlings grown under high temperature (28 °C), on media supplemented with or without sucrose. When grown in high temperature (28 °C) on the medium with sucrose, *ABP1-GFP*^{OE} exhibited longer hypocotyls compared to WT, whereas the hypocotyl length of *abp1* mutants was comparable to that of WT plants (Fig. 7D). At high

temperature (28 °C), but in absence, of sucrose the hypocotyl elongation of *ABP1-GFP*^{OE} line was less inhibited than in WT (Fig. 7E).

To test whether *ABP1* plays a role in wound healing responses, we performed a targeted cell ablation in the root tips of *abp1-TD1* and *ABP1-GFP*^{OE} lines [53,81]. After cell ablation, the numbers of initiating periclinal cell divisions in *abp1-TD1* and *ABP1-GFP*^{OE} were similar to that in WT (Fig. S3).

Taken together, the results show that the root growth of *abp1* loss-of-function mutants is not influenced differently by salt stress and high temperature. *ABP1* gain-of-function seedlings show increased hypocotyl growth when grown at high temperature.
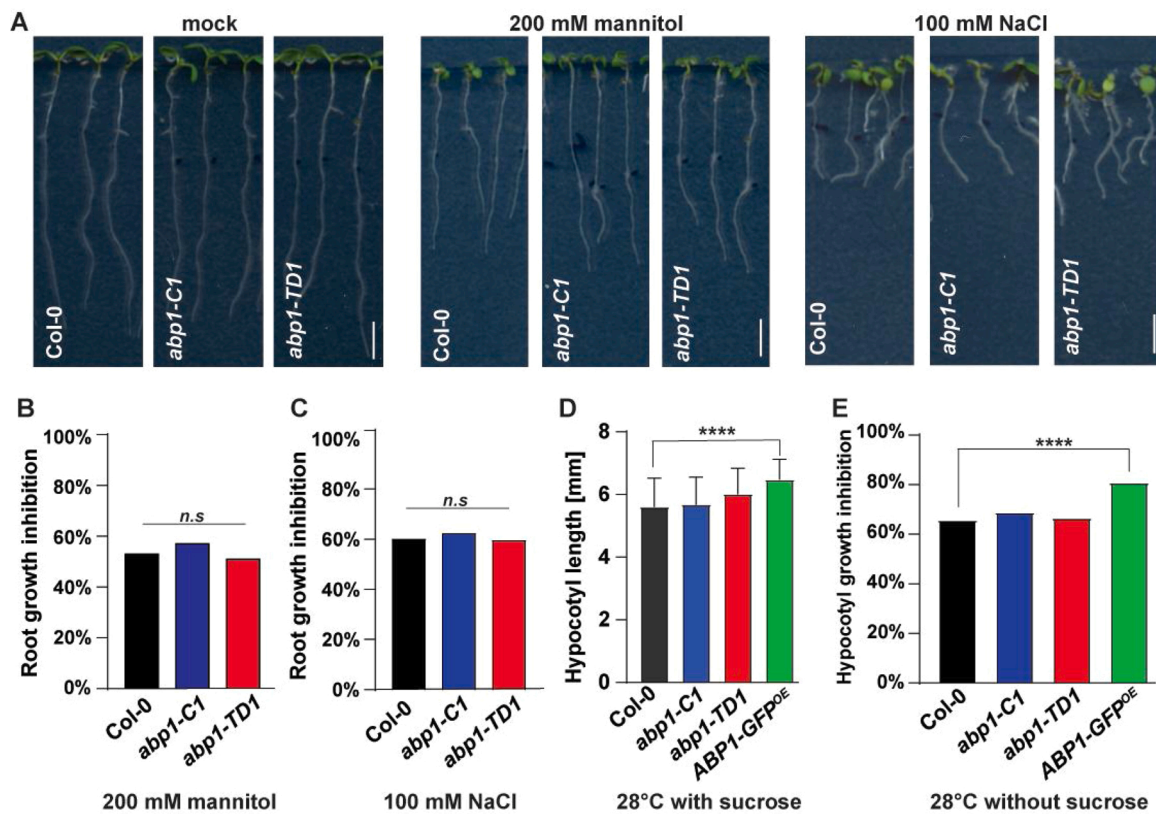
Fig. 7. Role of ABP1 during stress.

(A) Representative images of 8-d-old Col-0, *abp1-C1, abp1-TD1* and *ABP1-GFP*^{OE} seedlings grown for 4 days on control media or on media supplemented with either 200 mM mannitol or 100 mM NaCl. Scale bar =5 mm.

(B–C) Quantification of the root growth inhibition of Col-0, *abp1-C1* and *abp1-TD1* seedlings after treatment with 200 mM mannitol (B) or 100 mM NaCl (C). For each genotype, at least 10 roots were measured per experiment. The experiment was repeated 3 times with the similar results and the pooled values are presented. The statistical significance was tested by Wilcoxon test.

(D) Quantification of the hypocotyl length of 7-d-old Col-0, *abp1-C1, abp1-TD1* and *ABP1-GFP*^{OE} seedlings grown under continuous light, higher temperature (28 °C). For each genotype and experiment, at least 25 hypocotyls were analyzed. Error bars denote standard error. Asterisks indicate significant differences according to Student's t tests (****, P < 0. 0001). The experiment was repeated 3 times with the similar results.

(E) Quantification of the hypocotyl growth inhibition sucrose of Col-0, *abp1-C1, abp1-TD1* and *ABP1-GFP*^{OE} seedlings grown under continuous light, higher temperature (28 °C) and in absence of sucrose. For each genotype, at least 10 roots were measured per experiment. Asterisks indicate significant differences according to Student's t tests (****, P < 0. 0001). The experiment was repeated 3 times with the similar results and the pooled values are presented.

3.8. Role of ABP1 in rosette leaves and inflorescence development

The establishment of auxin maxima in the shoot apical meristem (SAM) and directed basipetal polar auxin transport are crucial for overall shoot development [59,82–86]. *ABP1* is expressed in both SAM and rosette leaves (Fig. S1B), therefore we investigated its possible function in shoot development.

First, we characterized leaf development. Visually, the size and shape of rosette leaves in *abp1* mutants and *ABP1-GFP*^{OE} plants were comparable to that of WT plants. We quantified the rosette leaves number at the stage when the first flower of each individual plant bloomed. We observed that the *apb1-TD1* mutant developed slightly more, whereas the *ABP1-GFP*^{OE} line developed significantly less rosette leaves in comparison to WT (Fig. 8A). However, the results for the *abp1-TD1* mutant line were variable between the experimental repetitions. We found no difference in the number of cauline leaves for any of the analyzed lines (Fig. S4A).

Further, we studied the function of *ABP1* during bolting. We measured the length of the first internode of *abp1* mutants and *ABP1-GFP*^{OE} and we recorded the timing to reach 1 cm. Compared to WT, both *abp1* mutants and *ABP1-GFP*^{OE} line bolt earlier, at 21st and 22nd day after sowing versus 23rd day in WT (Fig. 8B).

To determine whether *ABP1* is involved in phyllotaxis establishment,

we measured the sequence of divergence angles between siliques in *abp1* mutants. Visually, *abp1* mutants developed normal inflorescence stems (Fig. 8C). WT plants typically exhibit a spiral phyllotaxis that leads to a distribution of the consecutive organs on the stem with a divergence angle close to 137.5° [87]. Our analysis revealed that the distribution of divergence angles in *abp1* mutants was not altered (Fig. 8D–F). We also analyzed the internode length between the siliques and counted the number of rosette and cauline branches of *abp1* mutant and *ABP1-GFP*^{OE} plants. However, we did not detect any differences (Fig. S4B-D).

The results show that overexpression of *ABP1* affects the number of rosette leaves and that both *ABP1* loss- and gain-of-function accelerate bolting.

3.9. Role of ABP1 in auxin-mediated PIN polarization and BFA-visualized PIN trafficking

The formation of organized vasculature requires coordinated cell polarization. The canalization hypothesis proposes that auxin acts as a polarizing cue in this process [88] and that auxin feed-back on PIN polarity, together with constitutive PIN endocytic trafficking are important features in this process [54,89,90]. Since overexpression of *ABP1* results in defects in vascular tissue formation (Fig. 6B), we tested whether *abp1* loss- or gain-of-function alleles show defects in these
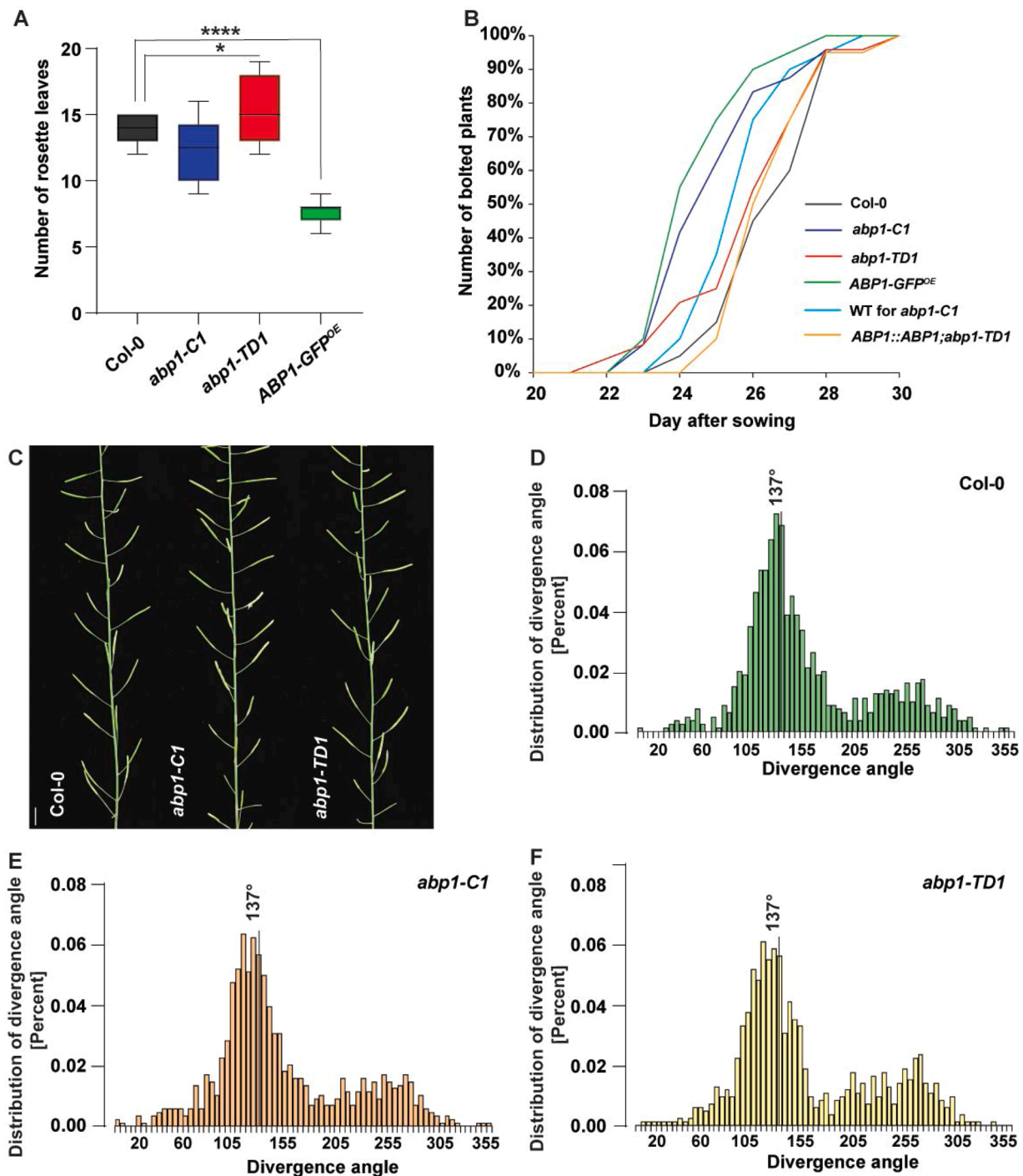
Fig. 8. Role of ABP1 in rosette leaves and inflorescence development.
(A) Boxplot showing the number of rosette leaves of Col-0, *abp1-C1*, *abp1-TD1* and *ABP1-GFP^{OE}* plants. For each genotype per experiment, at least 10 rosettes were scored when the first flower bloomed on each single plant. For box plot, box defines the first and third quartiles, and the central lines in the box represent the median. Whiskers, from minimum to maximum. Asterisks indicate significant differences according to Student's t tests (*, P < 0.05; ****, P < 0. 0001). The experiment was repeated 3 times with the similar result.
(B) Quantification of bolting time of Col-0, *abp1-C1*, *abp1-TD1*, *ABP1-GFP^{OE}*, WT for *abp1-C1*, and *ABP1::ABP1;abp1-TD1*. The graph shows number of plants with inflorescence stem ≥ 1 cm for the given day in percentage. For each genotype per experiment, at least 20 plants were scored. The experiment was at this given setup repeated 2 times with the similar result, and additionally 2 times for Col-0, *abp1-C1*, *abp1-TD1*, *ABP1-GFP^{OE}* with the similar result.
(C) Representative pictures of the inflorescence stem of Col-0, *abp1-C1*, and *abp1-TD1*. Scale bar =1 cm.
(D–F) Distribution of divergence angles between the siliques in Col-0, *abp1-C1*, and *abp1-TD1*. For each genotype divergence angles of 25 individual plants were measured.

processes. To evaluate the effect of auxin on PIN polarity, we analyzed the repolarization of PIN1 from the basal to the inner lateral side in root endodermis cells and the repolarization of PIN2 from the basal to the outer lateral side in root cortex cells [54] following auxin treatment in *abp1* mutants and *ABP1-GFP*[OE]. Anti-PIN1 and anti-PIN2 immunolocalization revealed that PIN1 and PIN2 repolarization was not altered in *abp1* mutants, while overexpression of ABP1 led to reduced or no repolarization of PIN1 and PIN2 respectively (Fig. 9A–B).

Further, we used the trafficking inhibitor Brefeldin A (BFA) to indirectly visualize PIN intracellular trafficking [91]. BFA treatment results in PIN internal aggregation manifested as BFA-body formation and this effect is decreased when BFA is used together with auxin [9]. The anti-PIN1 immunostaining in roots after BFA treatment showed that the intracellular aggregation of PIN1 was similar to that of WT in both *abp1* mutants (Fig. 9C) and [92]. In *ABP1-GFP*[OE] we observed repeatedly that BFA affected PIN1 intracellular aggregation more severely (BFA bodies were more pronounced) (Fig. 9C). Anti-PIN1 immunostaining after auxin and BFA co-treatment confirmed that auxin inhibited BFA-body formation. Comparison of the *abp1* mutants with the corresponding complemented lines did not reveal any consistent changes in the auxin effect on BFA-induced PIN1 aggregation, whereas *ABP1-GFP*[OE] showed again slightly more BFA-induced PIN1 aggregation even in presence of auxin (Fig. 9C). The analysis of the BFA effect on PIN2 intracellular aggregation revealed no consistent and reproducible differences in BFA-body formation between WT, *abp1* mutants and *ABP1-GFP*[OE] (Fig. 9D). Accordingly, auxin and BFA co-treatment led to a comparable and variable decrease of PIN2 intracellular aggregation in WT, *abp1* mutants and *ABP1-GFP*[OE] (Fig. 9D).

Taken together, the *ABP1* overexpression interferes with auxin-induced PIN repolarization and slightly affects BFA-induced, constitutive PIN1 but not PIN2 trafficking, while mutation in *ABP1* does not show altered auxin feed-back on PIN polarity or constitutive PIN recycling.

4. Discussion

ABP1 has been identified in maize decades ago based on its potential ability to bind auxin [93,94]. Nonetheless, the developmental roles and cellular functions of ABP1 remain unclear due to problems with some of the genetic material [35,39,40,42] and due to the lack of obvious developmental defects after superficial analyzes of the verified knock-out lines [38].

Here, we assessed the function of ABP1 in various developmental processes and (re)evaluated its role in cellular processes related to trafficking and polar distribution of PIN auxin transporters.

4.1. ABP1 is not essential for or regulated by TIR1/AFB-mediated auxin responses

ABP1 promoter activity has been reported to overlap, to some extent, with that of the transcriptional DR5 auxin reporter during early seedling development [43]. Our analysis revealed a similar overlap in hydathodes, root tips and lateral root primordia as well as in older seedlings. The activity of the *ABP1* promoter at places with high auxin response suggested either that auxin might regulate the transcription of *ABP1* or that ABP1 is somehow linked to TIR1/AFB-mediated transcriptional auxin signaling.

Indeed, *ABP1* was previously identified among early auxin-regulated genes. *ABP1* transcription was upregulated by auxin in a dose dependent manner within 30 min in 19-d-old WT seedlings [95]. Our observations in 5-d-old WT roots and shoots did not reveal any changes in *ABP1* expression following auxin treatment. These contradictory findings suggest that a potential auxin effect on *ABP1* transcription could be tissue- and/or developmental stage-dependent.

Also, the connection between *ABP1* and TIR1/AFB-mediated auxin signaling was previously investigated. Downregulation of the *ABP1*

activity was shown to affect transcription of auxin-responsive genes [33, 95,96], to regulate Aux/IAA homeostasis and thus negatively impact on the SCF[TIR1/AFB] pathway [97]. However, these observations are inconclusive due to the potential off-targets in the conditional knock-down lines [42] and the inactivation of *ABP1* did not have any significant effects on the DR5 auxin response reporter activity [33]. In the verified *abp1* knock-out lines it was reported that auxin-regulated gene expression is unchanged [38] and our analysis in these lines and following *ABP1* overexpression in protoplasts did also not reveal any changes in DR5 reporter activity. Furthermore, *abp1* knock-out lines also showed normal TIR1/AFB-mediated non-transcriptional auxin effect on root growth. Overall, these observations suggest that *ABP1* is not directly involved in the TIR1/AFB-mediated auxin response.

4.2. ABP1 loss-of-function mutants show minor defects in development

The initial analysis of CRISPR and T-DNA insertion *abp1* knock-out mutants did not reveal any obvious defects during development under normal conditions leading to a conclusion that *ABP1* is not required for Arabidopsis development [38]. We analyzed different auxin-related phenotypes of the corresponding *abp1* knock-out mutants in more detail. We observed that both *abp1* alleles exhibited normal root growth, etiolated hypocotyl, root and shoot gravitropic responses, lateral root and leaf development, including venation and phyllotaxis. Notably, both *abp1* mutant alleles bolted earlier compared to the control lines. Accelerated bolting in *abp1* mutants might be caused by changes in auxin levels caused by either impaired biosynthesis, auxin transport or eventually a change in auxin sensitivity. Nonetheless, it is unclear why such changes are not reflected also in other developmental processes regulated by auxin.

4.3. ABP1 gain-of-function lines show a plethora of auxin-related phenotypes

ABP1 overexpression has been shown previously to cause several postembryonic developmental defects [5,10,35,98,99]. Similarly, our analysis of a stable line expressing *35S::ABP1-GFP* revealed that *ABP1* gain-of-function leads to developmental changes. Seedlings overexpressing *ABP1* have reduced root length, impaired auxin-induced lateral root development, enhanced elongation of both high temperature- and dark-grown hypocotyls, reduced root and shoot gravitropic response, defective vasculature development, increased size of young rosettes but decreased number of rosettes leaves. Additionally, similar to the *abp1* mutants, *ABP1* overexpressors also bolted earlier. At the cellular level, we confirmed the previous observations [10,35] that the *ABP1* gain-of-function affects the BFA-sensitive PIN endocytic trafficking and newly showed that they also impair auxin effects on PIN polar distribution in root cells.

All aforementioned processes, which were found defective in *ABP1* gain-of-function mutants are linked to auxin regulation. It is therefore conceivable that, in line with the importance of the auxin binding pocket for the *ABP1* function [35], *ABP1* plays so far a mechanistically unclear role in auxin perception and signaling.

4.4. Potential role and functional mechanism of Arabidopsis ABP1

Arabidopsis *ABP1* was identified based on the orthology with *ABP1* previously found in maize [98,100]. Auxin-binding properties of maize ABP1 are well characterized. Several biochemical studies along with the structural analysis of the ABP1-auxin co-crystal revealed that maize ABP1 binds auxin with the highest affinity at apoplastic pH 5.5, while binding at pH 7.2 corresponding to the ER lumen where the majority of protein is localized, is much lower [26–29,94,101]. In contrast, the auxin-binding properties of Arabidopsis ABP1 have not been characterized yet. Based on the high homology with the maize protein, it is assumed that Arabidopsis ABP1 binds auxin in a similar manner. This
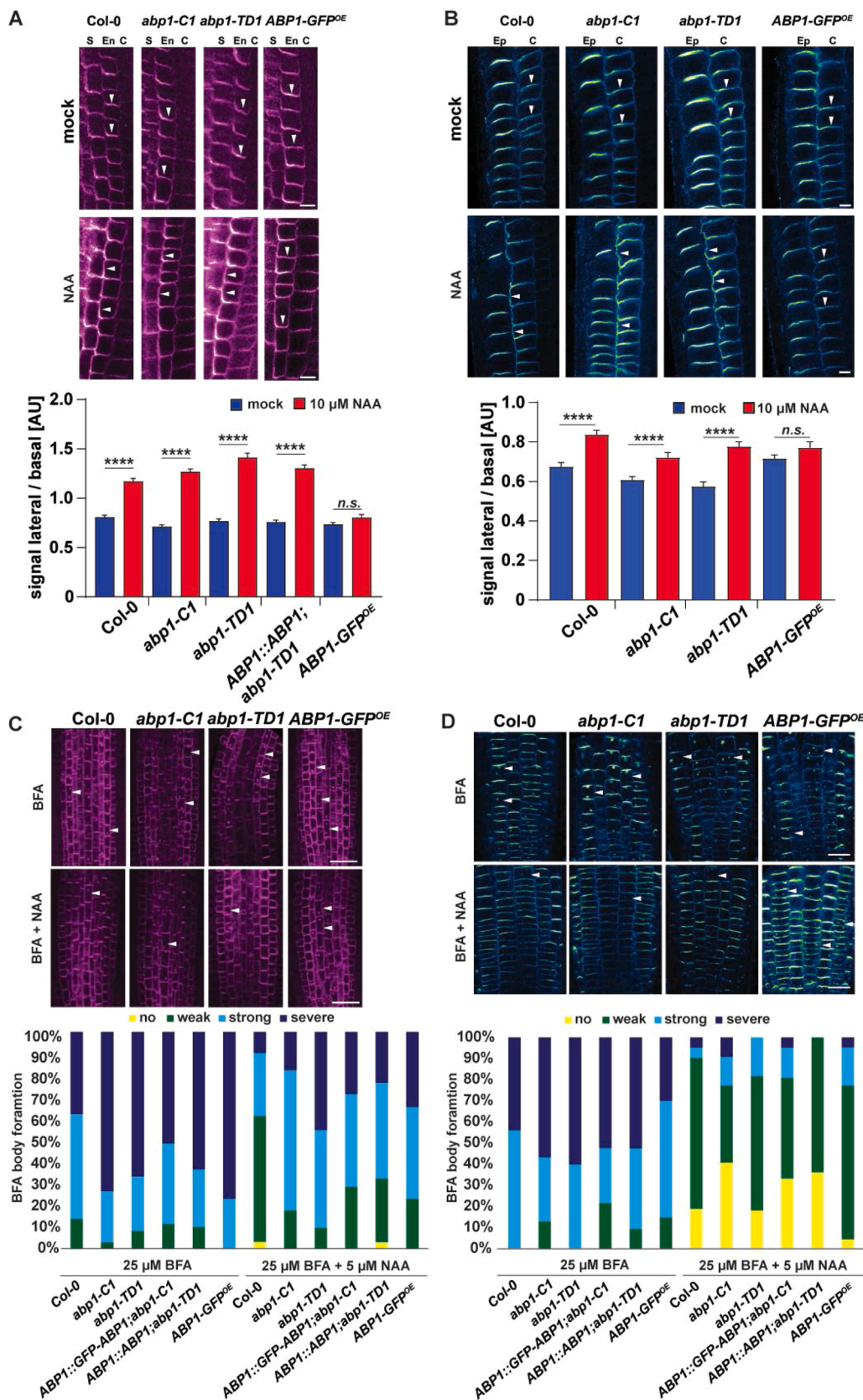
Fig. 9. Role of ABP1 in auxin-mediated PIN polarization and BFA-visualized PIN trafficking.

(A) Representative pictures of PIN1 immunolocalization in root meristem of 4-d-old Col-0, *abp1-C1*, *abp1-TD1* and *ABP1-GFP^OE* after mock (upper panel) and 4 h 10μM NAA treatment (lower panel). Scale bar =5 μm. The letters indicate an appropriate cell file - S (stele), En (endodermis), C (cortex). Arrow heads point to basal/lateral PIN1 localization in endodermis. The quantitative evaluation shows mean ratio of PIN1 lateral-to-basal signal intensity ratio in endodermis cells of Col-0, *abp1-C1*, *abp1-TD1*, *ABP1::ABP1;abp1-TD1* and *ABP1-GFP^OE*. Error bars denote standard error. Asterisks indicate significant differences according to Student's t tests (****, P < 0. 0001). The experiment was repeated 3 times, one representative experiment is presented.

(B) Representative pictures of PIN2 immunolocalization in root meristem of 4-d-old Col-0, *abp1-C1*, *abp1-TD1* and *ABP1-GFP^OE* after mock (upper panel) and 4 h 10μM NAA treatment (lower panel). Scale bar =5 μm. The letters indicate an appropriate cell file – Ep (epidermis), C (cortex). Arrow heads point to basal/lateral PIN2 localization in cortex. The quantitative evaluation shows mean ratio of PIN2 lateral-to-basal signal intensity ratio in cortex cells of Col-0, *abp1-C1*, *abp1-TD1* and *ABP1-GFP^OE*. Error bars denote standard error. Asterisks indicate significant differences according to Student's t tests (****, P < 0. 0001). The experiment was repeated 3 times, one representative experiment is presented.

(C) Representative pictures of PIN1 immunolocalization in primary root stele of 4-d-old Col-0, *abp1-C1*, *abp1-TD1* and *ABP1-GFP^OE* after 1 h 25 μM BFA treatment (upper panel) and after 30 min 5 μM NAA pre-treatment followed by 1 h 25 μM BFA and 5 μM NAA co-treatment (lower panel). Arrow heads point to affected cells. Scale bar =20 μm. The quantitative evaluation shows the scoring of an overall count of formed BFA bodies in Col-0, *abp1-C1*, *abp1-TD1*, *ABP1::GFP-ABP1;abp1-C1*, *ABP1::ABP1;abp1-TD1* and *ABP1-GFP^OE*. At least 8 roots were scored for each genotype and experiment. The pooled result of 3 independent experiments is presented.

(D) Representative pictures of PIN2 immunolocalization in primary root epidermis of 4-d-old Col-0, *abp1-C1*, *abp1-TD1* and *ABP1-GFP^OE* after 1 h 25 μM BFA treatment (upper panel) and after 30 min 5 μM NAA pre-treatment followed by 1 h 25 μM BFA and 5 μM NAA co-treatment (lower panel). Arrow heads point to affected cells. Scale bar =20 μm. The quantitative evaluation shows the scoring of an overall count of formed BFA bodies in Col-0, *abp1-C1*,

statement is supported by the finding that the auxin-binding pocket of Arabidopsis ABP1 is important for its gain-of-function cellular and developmental roles [35].

The ABP1 binding optimum at pH 5.5 would imply that ABP1 is functional in the apoplast, further supported by auxin-dependent interaction between ABP1 and the plasma membrane-localized receptor-like kinase TMK1 [30,31]. TMK1 belongs to a four-member TMK receptor-like kinase family, that function redundantly and multiple mutants show severe reduction in organ size and substantial growth retardation [20]. Both TMK1 and TMK4 play roles in auxin-mediated developmental processes and in the control of local auxin biosynthesis [22,23,30]. Importantly, TMK1 mediates auxin signaling that regulates differential growth of the apical hook [21]. However, the mechanism of how TMK1 perceives auxin remains elusive.

The function of ABP1 as a part of the auxin perception machinery contributing towards TMK-based downstream signaling, is a tempting hypothesis consistent with a rather broad spectrum of auxin-related growth defects. But it is not supported by the rather mild phenotypic defects in the *abp1* loss-of-function mutants, especially considering that *ABP1* is a single copy gene in Arabidopsis [100]. On the other hand, *ABP1* is evolutionary conserved and ubiquitous in vascular plants [102], suggesting that it has an important and conserved function. Structurally ABP1 belongs to an ancient group of germin and germin-like proteins that have a highly conserved tertiary structure despite low similarity in primary sequence among the members [28,103]. Therefore, it is possible that some other proteins from the germin family are functionally redundant with ABP1, thus masking the effect of the *abp1* mutation. Nonetheless, to identify and characterize functional homologues within this large family will be a challenging task. An alternative explanation for the weak developmental defects in *abp1* loss-of-function mutants is that *ABP1* plays an important role in specific processes that provide competitive advantage in nature but are not easily manifested under laboratory conditions.

5. Conclusions

In conclusion, our detailed phenotypic analysis of both *ABP1* gain- and loss-of-function lines provides new insights into the developmental role of *ABP1*. Despite the overlap of *ABP1* expression pattern with auxin response maxima during seedling development, none of our observations supports a direct involvement of *ABP1* in the TIR1/AFB-mediated transcriptional auxin response. *abp1* knock-out mutants show only mild phenotypic defects, whereas *ABP1* overexpression generates a broad range of potentially auxin-related phenotypes. The previously described strong and related defects in conditional *abp1* knock-down lines let us hypothesize that the discrepancy between the effects of loss- and gain-of-function is due to the action of unknown germin family proteins that are functionally redundant with ABP1.

Author contribution

Z.G., Mi.Ga., M.P., X.Z., Ma.Gl., L.L., J.M., I.V., H.H., J.H., M.Č., M. Z., L.H., M.F., T.V. and J.F. designed and conducted experiments and analyzed data. G.B. and Z.P. helped with performing experiments. R.H. and I.V. developed RG-tracker. Z.G., L.H. and T.X. contributed with the generation of the genetic material. Z.G., X.Z., Mi.Ga. and J.F. wrote the manuscript.

Declaration of Competing Interest

The authors report no declarations of interest.

Acknowledgments

Appendix A. Supplementary data

Supplementary material related to this article can be found, in the online version, at doi:https://doi.org/10.1016/j.plantsci.2020.110750.

References

[1] J. Brumos, L.M. Robles, J. Yun, T.C. Vu, S. Jackson, J.M. Alonso, A.N. Stepanova, Local auxin biosynthesis is a key regulator of plant development, Dev. Cell 47 (2018) 306–318, https://doi.org/10.1016/j.devcel.2018.09.022, e5.

[2] M. Adamowski, J. Friml, PIN-dependent auxin transport: action, regulation, and evolution, Plant Cell 27 (2015) 20–32, https://doi.org/10.1105/tpc.114.134874.

[3] B.O. Bargmann, S. Vanneste, G. Krouk, T. Nawy, I. Efroni, E. Shani, G. Choe, J. Friml, D.C. Bergmann, M. Estelle, K.D. Birnbaum, I.D.B. Inte, A Map of Cell Type-specific Auxin Responses, 2013, pp. 1–13, https://doi.org/10.1038/msb.2013.40.

[4] D. Weijers, D. Wagner, Transcriptional responses to the auxin hormone, Annu. Rev. Plant Biol. 67 (2016) 539–574, https://doi.org/10.1146/annurev-arplant-043015-112122.

[5] B. Steffens, C. Feckler, K. Palme, M. Christian, M. Böttger, H. Lüthen, The auxin signal for protoplast swelling is perceived by extracellular ABP1, Plant J. 27 (2001) 591–599, https://doi.org/10.1046/j.1365-313X.2001.01103.x.

[6] R.I. Dahlke, S. Fraas, K.K. Ullrich, K. Heinemann, M. Romeiks, T. Rickmeyer, G. Klebe, K. Palme, H. Lüthen, B. Steffens, Protoplast swelling and hypocotyl growth depend on different auxin signaling pathways, Plant Physiol. 175 (2017) 982–994, https://doi.org/10.1104/pp.17.00733.

[7] G.B. Monshausen, N.D. Miller, A.S. Murphy, S. Gilroy, Dynamics of auxin-dependent Ca 2+ and pH signaling in root growth revealed by integrating high-resolution imaging with automated computer vision-based analysis, Plant J. 65 (2011) 309–318, https://doi.org/10.1111/j.1365-313X.2010.04423.x.

[8] H.W. Shih, C.L. Depew, N.D. Miller, G.B. Monshausen, The cyclic nucleotide-gated channel CNGC14 regulates root gravitropism in arabidopsis thaliana, Curr. Biol. 25 (2015) 3119–3125, https://doi.org/10.1016/j.cub.2015.10.025.

[9] T. Paciorek, E. Zazímalová, N. Ruthardt, J. Petrásek, Y.-D. Stierhof, J. Kleine-Vehn, D.A. Morris, N. Emans, G. Jürgens, N. Geldner, J. Friml, Auxin inhibits endocytosis and promotes its own efflux from cells, Nature 435 (2005) 1251–1256, https://doi.org/10.1038/nature03633.

[10] S. Robert, J. Kleine-Vehn, E. Barbez, M. Sauer, T. Paciorek, P. Baster, S. Vanneste, J. Zhang, S. Simon, M. Čovanová, K. Hayashi, P. Dhonukshe, Z. Yang, S. Y. Bednarek, A.M. Jones, C. Luschnig, F. Aniento, E. Zažímalová, J. Friml, ABP1 mediates auxin inhibition of clathrin-dependent endocytosis in arabidopsis, Cell 143 (2010) 111–121, https://doi.org/10.1016/j.cell.2010.09.027.

[11] M. Kubeš, R. Napier, Non-canonical auxin signalling: fast and curious, J. Exp. Bot. 70 (2019) 2609–2614, https://doi.org/10.1093/jxb/erz111.

[12] M. Gallei, C. Luschnig, J. Friml, Auxin signalling in growth: schrödinger's cat out of the bag, Curr. Opin. Plant Biol. 53 (2020) 43–49, https://doi.org/10.1016/j.pbi.2019.10.003.

[13] O. Leyser, Auxin signaling, Plant Physiol. 176 (2018) 465–479, https://doi.org/10.1104/pp.17.00765.

[14] A.K. Spartz, S.H. Lee, J.P. Wenger, N. Gonzalez, H. Itoh, D. Inzé, W.A. Peer, A.S. Murphy, P.J. Overvoorde, W.M. Gray, The SAUR19 subfamily of SMALL AUXIN UP RNA genes promote cell expansion, Plant J. 70 (2012) 978–990, https://doi.org/10.1111/j.1365-313X.2012.04946.x.

[15] M. Fendrych, J. Leung, J. Friml, Tir1/AFB-Aux/IAA auxin perception mediates rapid cell wall acidification and growth of Arabidopsis hypocotyls, Elife 5 (2016) 1–18, https://doi.org/10.7554/eLife.19048.

[16] M. Fendrych, M. Akhmanova, J. Merrin, M. Glanc, S. Hagihara, K. Takahashi, N. Uchida, K.U. Torii, J. Friml, Rapid and reversible root growth inhibition by TIR1 auxin signalling, Nat. Plants 4 (2018) 453–459, https://doi.org/10.1038/s41477-018-0190-1.

[17] J. Dindas, S. Scherzer, M.R.G. Roelfsema, K. Von Meyer, H.M. Müller, K.A.S. Al-Rasheid, K. Palme, P. Dietrich, D. Becker, M.J. Bennett, R. Hedrich, AUX1-mediated root hair auxin influx governs SCFTIR1/AFB-type Ca2+ signaling, Nat. Commun. 9 (2018), https://doi.org/10.1038/s41467-018-03582-5.

[18] S. Simonini, J. Deb, L. Moubayidin, P. Stephenson, M. Valluru, A. Freire-Rios, K. Sorefan, D. Weijers, J. Friml, L. Østergaard, A noncanonical auxin-sensing mechanism is required for organ morphogenesis in arabidopsis, Genes Dev. 30 (2016) 2286–2296, https://doi.org/10.1101/gad.285361.116.

[19] A. Kuhn, S.R. Harborough, H.M. McLaughlin, B. Natarajan, I. Verstraeten, J. Friml, S. Kepinski, L. Østergaard, Direct ETTIN-auxin interaction controls chromatin states in gynoecium development, Elife 9 (2020) 1–18, https://doi.org/10.7554/eLife.51787.

[20] N. Dai, W. Wang, S.E. Patterson, A.B. Bleecker, The TMK subfamily of receptor-like kinases in Arabidopsis display an essential role in growth and a reduced sensitivity to auxin, PLoS One 8 (2013) 1–12, https://doi.org/10.1371/journal.pone.0060990.

[21] M. Cao, R. Chen, P. Li, Y. Yu, R. Zheng, D. Ge, W. Zheng, X. Wang, Y. Gu, Z. Gelová, J. Friml, H. Zhang, R. Liu, J. He, T. Xu, TMK1-mediated auxin signalling regulates differential growth of the apical hook, Nature 568 (2019) 240–243, https://doi.org/10.1038/s41586-019-1069-7.

[22] R. Huang, R. Zheng, J. He, Z. Zhou, J. Wang, Y. Xiong, T. Xu, Noncanonical auxin signaling regulates cell division pattern during lateral root development, Proc. Natl. Acad. Sci. U. S. A. 116 (2019) 21285–21290, https://doi.org/10.1073/pnas.1910916116.

[23] Q. Wang, G. Qin, M. Cao, R. Chen, Y. He, L. Yang, Z. Zeng, Y. Yu, Y. Gu, W. Xing, W.A. Tao, T. Xu, A phosphorylation-based switch controls TAA1-mediated auxin biosynthesis in plants, Nat. Commun. 11 (2020), https://doi.org/10.1038/s41467-020-14395-w.

[24] N. Leblanc, C. Roux, J.M. Pradier, C. Perrot-Rechenmann, Characterization of two cDNAs encoding auxin-binding proteins in Nicotiana tabacum, Plant Mol. Biol. 33 (1997) 679–689, https://doi.org/10.1023/a:1005757815212.

[25] S. Watanabe, S. Shimomura, Cloning and expression of two genes encoding auxin-binding proteins from tobacco, Plant Mol. Biol. 36 (1998) 63–74, https://doi.org/10.1023/A:1005999821066.

[26] H. Tian, D. Klambt, A.M. Jones, Auxin-binding protein 1 does not bind auxin within the endoplasmic reticulum despite this being the predominant subcellular location for this hormone receptor, J. Biol. Chem. 270 (1995) 26962–26969, https://doi.org/10.1074/jbc.270.45.26962.

[27] N. Leblanc, K. David, J. Grosclaude, J.M. Pradier, H. Barbier-Brygoo, S. Labiau, C. Perrot-Rechenmann, A novel immunological approach establishes that the auxin-binding protein, Nt-abp1, is an element involved in auxin signaling at the plasma membrane, J. Biol. Chem. 274 (1999) 28314–28320, https://doi.org/10.1074/jbc.274.40.28314.

[28] E.J. Woo, J. Marshall, J. Bauly, J.G. Chen, M. Venis, R.M. Napier, R.W. Pickersgill, Crystal structure of auxin-binding protein 1 in complex with auxin, EMBO J. 21 (2002) 2877–2885, https://doi.org/10.1093/emboj/cdf291.

[29] A.M. Jones, E.M. Herman, KDEL-containing auxin-binding protein is secreted to the plasma membrane and cell wall, Plant Physiol. 101 (1993) 595–606, https://doi.org/10.1104/pp.101.2.595.

[30] T. Xu, M. Wen, S. Nagawa, Y. Fu, J.-G. Chen, M.-J. Wu, C. Perrot-Rechenmann, J. Friml, A.M. Jones, Z. Yang, Cell surface- and rho GTPase-based auxin signaling controls cellular interdigitation in Arabidopsis, Cell 143 (2010) 99–110, https://doi.org/10.1016/j.cell.2010.09.003.

[31] T. Xu, N. Dai, J. Chen, S. Nagawa, M. Cao, H. Li, Z. Zhou, X. Chen, R. De Rycke, H. Rakusová, W. Wang, A.M. Jones, J. Friml, S.E. Patterson, A.B. Bleecker, Z. Yang, Cell surface ABP1-TMK auxin-sensing complex activates ROP GTPase signaling, Science 343 (2014) 1025–1028, https://doi.org/10.1126/science.1245125.

[32] P. Grones, J. Friml, Auxin transporters and binding proteins at a glance, J. Cell. Sci. 128 (2015) 1–7, https://doi.org/10.1242/jcs.159418.

[33] A. Tromas, N. Braun, P. Muller, T. Khodus, I.A. Paponov, K. Palme, K. Ljung, J.Y. Lee, P. Benfey, J.A.H. Murray, B. Scheres, C. Perrot-Rechenmann, The AUXIN BINDING PROTEIN 1 is required for differential Auxin responses mediating root growth, PLoS One 4 (2009) 1–11, https://doi.org/10.1371/journal.pone.0006648.

[34] X. Chen, S. Naramoto, S. Robert, R. Tejos, C. Löfke, D. Lin, Z. Yang, J. Friml, ABP1 and ROP6 GTPase signaling regulate clathrin-mediated endocytosis in Arabidopsis roots, Curr. Biol. 22 (2012) 1326–1332, https://doi.org/10.1016/j.cub.2012.05.020.

[35] P. Grones, X. Chen, S. Simon, W.A. Kaufmann, R. De Rycke, T. Nodzyński, E. Zažímalová, J. Friml, Auxin-binding pocket of ABP1 is crucial for its gain-of-function cellular and developmental roles, J. Exp. Bot. 66 (2015) 5055–5065, https://doi.org/10.1093/jxb/erv177.

[36] X. Chen, L. Grandont, H. Li, R. Hauschild, S. Paque, A. Abuzeineh, H. Rakusová, E. Benkova, C. Perrot-Rechenmann, J. Friml, Inhibition of cell expansion by rapid ABP1-mediated auxin effect on microtubules, Nature 516 (2014) 90–93, https://doi.org/10.1038/nature13889.

[37] S. Paque, G. Mouille, L. Grandont, D. Alabadí, C. Gaertner, A. Goyallon, P. Muller, C. Primard-Brisset, R. Sormani, M.A. Blázquez, C. Perrot-Rechenmann, AUXIN BINDING PROTEIN1 links cellwall remodeling, auxin signaling, and cell expansion in Arabidopsis, Plant Cell 26 (2014) 280–295, https://doi.org/10.1105/tpc.113.120048.

[38] Y. Gao, Y. Zhang, D. Zhang, X. Dai, M. Estelle, Y. Zhao, Auxin binding protein 1 (ABP1) is not required for either auxin signaling or Arabidopsis development, Proc. Natl. Acad. Sci. U. S. A. 112 (2015) 2275–2280, https://doi.org/10.1073/pnas.1500365112.

[39] J. Michalko, M. Dravecká, T. Bollenbach, J. Friml, Embryo-lethal phenotypes in early abp1 mutants are due to disruption of the neighboring BSM gene [version 1; referees: 3 approved], F1000Research 4 (2015), https://doi.org/10.12688/f1000research.7143.1.

[40] X. Dai, Y. Zhang, D. Zhang, J. Chen, X. Gao, M. Estelle, Y. Zhao, Embryonic lethality of Arabidopsis abp1-1 is caused by deletion of the adjacent BSM gene, Nat. Plants 1 (2015) 3–6, https://doi.org/10.1038/nplants.2015.183.

[41] T.A. Enders, S. Oh, Z. Yang, B.L. Montgomery, L.C. Strader, Genome sequencing of arabidopsis abp1-5 reveals second-site mutations that may affect phenotypes, Plant Cell 27 (2015) 1820–1826, https://doi.org/10.1105/tpc.15.00214.

[42] J. Michalko, M. Glanc, C. Perrot-Rechenmann, J. Friml, Strong morphological defects in conditional Arabidopsis abp1 knock-down mutants generated in absence of functional ABP1 protein, F1000Research 5 (2016) 86, https://doi.org/10.12688/f1000research.7654.1.

[43] M. Klode, R.I. Dahlke, M. Sauter, B. Steffens, Expression and subcellular localization of Arabidopsis thaliana auxin-binding protein 1 (ABP1), J. Plant Growth Regul. 30 (2011) 416–424, https://doi.org/10.1007/s00344-011-9203-2.

[44] J. Friml, A. Vieten, M. Sauer, D. Weijers, H. Schwarz, T. Hamann, R. Offringa, G. Jürgens, Efflux-dependent auxin gradients establish the apical-basal axis of Arabidopsis, Nature 426 (2003) 147–153, https://doi.org/10.1038/nature02085.

[45] S.J. Clough, A.F. Bent, Floral dip: a simplified method for Agrobacterium-mediated transformation of Arabidopsis thaliana, Plant J. 16 (1998) 735–743, https://doi.org/10.1046/j.1365-313x.1998.00343.x.

[46] J.E. Malamy, P.N. Benfey, Organization and cell differentiation in lateral roots of Arabidopsis thaliana, Development 124 (1997) 33–44.

[47] T. Czechowski, M. Stitt, T. Altmann, M.K. Udvardi, W.-R. Scheible, Genome-Wide Identification and Testing of Superior Reference Genes for Transcript Normalization in Arabidopsis, Plant Physiol. 139 (2005) 5 LP–17, https://doi.org/10.1104/pp.105.063743.

[48] D. von Wangenheim, R. Hauschild, M. Fendrych, V. Barone, E. Benková, J. Friml, Live tracking of moving samples in confocal microscopy for vertically grown roots, Elife 6 (2017), https://doi.org/10.7554/eLife.26792.

[49] J. Mathur, C. Koncz, Callus culture and regeneration, Methods Mol. Biol. 82 (1998) 31–34, https://doi.org/10.1385/0-89603-391-0:31.

[50] T. Ulmasov, J. Murfett, G. Hagen, T.J. Guilfoyle, Creation of a highly active synthetic AuxRE, Society 9 (1997) 1963–1971, https://doi.org/10.1105/tpc.9.11.1963.

[51] C. Després, C. Chubak, A. Rochon, R. Clark, T. Bethune, D. Desveaux, P.R. Fobert, The Arabidopsis NPR1 disease resistance protein is a novel cofactor that confers redox regulation of DNA binding activity to the basic domain/leucine zipper transcription factor TGA1, Plant Cell 15 (2003) 2181–2191, https://doi.org/10.1105/tpc.012849.

[52] S. Berg, D. Kutra, T. Kroeger, C.N. Straehle, B.X. Kausler, C. Haubold, M. Schiegg, J. Ales, T. Beier, M. Rudy, K. Eren, J.I. Cervantes, B. Xu, F. Beuttenmueller, A. Wolny, C. Zhang, U. Koethe, F.A. Hamprecht, A. Kreshuk, Ilastik: interactive machine learning for (Bio)image analysis, Nat. Methods 16 (2019) 1226–1232, https://doi.org/10.1038/s41592-019-0582-9.

[53] L. Hoermayer, J.C. Montesinos, P. Marhava, E. Benková, S. Yoshida, J. Friml, Wounding-induced changes in cellular pressure and localized auxin signalling spatially coordinate restorative divisions in roots, Proc. Natl. Acad. Sci. (2020), https://doi.org/10.1073/pnas.2003346117, 202003346.

[54] M. Sauer, J. Balla, C. Luschnig, J. Wisniewska, V. Reinöhl, J. Friml, E. Benková, Canalization of auxin flow by Aux/IAA-ARF-dependent feedback regulation of PIN polarity, Genes Dev. 20 (2006) 2902–2911, https://doi.org/10.1101/gad.390806.

[55] I. Abas, R. Benjamins, N. Malenica, T.T. Paciorek, J. Wiśniewska, J.C. Moulinier-Anzola, T. Sieberer, J. Friml, C. Luschnig, Intracellular trafficking and proteolysis of the Arabidopsis auxin-efflux facilitator PIN2 are involved in root gravitropism, Nat. Cell Biol. 8 (2006) 249–256, https://doi.org/10.1038/ncb1369.

[56] T. Hruz, O. Laule, G. Szabo, F. Wessendorp, S. Bleuler, L. Oertle, P. Widmayer, W. Gruissem, P. Zimmermann, Genevestigator V3: a reference expression database for the meta-analysis of transcriptomes, Adv. Bioinformatics 2008 (2008) 420747, https://doi.org/10.1155/2008/420747.

[57] S. Sabatini, D. Beis, H. Wolkenfelt, J. Murfett, T. Guilfoyle, J. Malamy, P. Benfey, O. Leyser, N. Bechtold, P. Weisbeek, B. Scheres, An auxin-dependent distal organizer of pattern and polarity in the Arabidopsis root, Cell 99 (1999) 463–472, https://doi.org/10.1016/s0092-8674(00)81535-4.

[58] J. Friml, E. Benková, I. Blilou, J. Wisniewska, T. Hamann, K. Ljung, S. Woody, G. Sandberg, B. Scheres, G. Jürgens, K. Palme, AtPIN4 mediates sink-driven auxin gradients and root patterning in Arabidopsis, Cell 108 (2002) 661–673, https://doi.org/10.1016/S0092-8674(02)00656-6.

[59] E. Benková, M. Michniewicz, M. Sauer, T. Teichmann, D. Seifertová, G. Jürgens, J. Friml, Local, efflux-dependent auxin gradients as a common module for plant

organ formation, Cell 115 (2003) 591–602, https://doi.org/10.1016/S0092-8674(03)00924-3.

[60] W. He, J. Brumos, H. Li, Y. Ji, M. Ke, X. Gong, Q. Zeng, W. Li, X. Zhang, F. An, X. Wen, P. Li, J. Chu, X. Sun, C. Yan, N. Yan, D.Y. Xie, N. Raikhel, Z. Yang, A. N. Stepanova, J.M. Alonso, H. Guo, A small-molecule screen identifies L-Kynurenine as a competitive inhibitor of TAA1/TAR activity in ethylene-directed auxin biosynthesis and root growth in Arabidopsis, Plant Cell 23 (2011) 3944–3960, https://doi.org/10.1105/tpc.111.089029.

[61] M. Lavy, M. Estelle, Mechanisms of auxin signaling, Development 143 (2016) 3226–3229, https://doi.org/10.1242/dev.131870.

[62] Z. Ding, J. Friml, Auxin regulates distal cell differentiation in Arabidopsis roots, Proc. Natl. Acad. Sci. U. S. A. 107 (2010) 12046–12051, https://doi.org/10.1073/pnas.1000672107.

[63] M.L. Evans, H. Ishikawa, M.A. Estelle, Responses of Arabidopsis roots to auxin studied with high temporal resolution: comparison of wild type and auxin-response mutants, Planta 194 (1994) 215–222, https://doi.org/10.1007/BF00196390.

[64] H.M.O. Leyser, F.B. Pickett, S. Dharmasiri, M. Estelle, Mutations in the AXR3 gene of Arabidopsis result in altered auxin response including ectopic expression from the SAUR-AC1 promoter, Plant J. 10 (1996) 403–413, https://doi.org/10.1046/j.1365-313x.1996.10030403.x.

[65] K. Scheitz, H. Lüthen, D. Schenck, Rapid auxin-induced root growth inhibition requires the TIR and AFB auxin receptors, Planta 238 (2013) 1171–1176, https://doi.org/10.1007/s00425-013-1941-x.

[66] C. Luschnig, R.A. Gaxiola, P. Grisafi, G.R. Fink, EIR1, a root-specific protein involved in auxin transport, is required for gravitropism in Arabidopsis thaliana, Genes Dev. 12 (1998) 2175–2187, https://doi.org/10.1101/gad.12.14.2175.

[67] H. Rakusová, M. Fendrych, J. Friml, Intracellular trafficking and PIN-mediated cell polarity during tropic responses in plants, Curr. Opin. Plant Biol. 23 (2015) 116–123, https://doi.org/10.1016/j.pbi.2014.12.002.

[68] S.H. Su, N.M. Gibbs, A.L. Jancewicz, P.H. Masson, Molecular mechanisms of root gravitropism, Curr. Biol. 27 (2017) R964–R972, https://doi.org/10.1016/j.cub.2017.07.015.

[69] H. Han, H. Rakusová, I. Verstraeten, Y. Zhang, J. Friml, SCF TIR1 / AFB auxin signaling for bending termination, Plant Physiol. Prev. 183 (2020) 37–40, https://doi.org/10.1104/pp.20.00212.

[70] W.M. Gray, A. Östin, G. Sandberg, C.P. Romano, M. Estelle, High temperature promotes auxin-mediated hypocotyl elongation in Arabidopsis, Proc. Natl. Acad. Sci. U. S. A. 95 (1998) 7197–7202, https://doi.org/10.1073/pnas.95.12.7197.

[71] A. Peaucelle, R. Wightman, H. Höfte, The control of growth symmetry breaking in the Arabidopsis hypocotyl, Curr. Biol. 25 (2015) 1746–1752, https://doi.org/10.1016/j.cub.2015.05.022.

[72] K. Takahashi, K.I. Hayashi, T. Kinoshita, Auxin activates the plasma membrane H +-ATPase by phosphorylation during hypocotyl elongation in Arabidopsis, Plant Physiol. 159 (2012) 632–641, https://doi.org/10.1104/pp.112.196428.

[73] E. Scarpella, D. Marcos, J. Friml, T. Berleth, Control of leaf vascular patterning by polar auxin transport, Genes Dev. 20 (2006) 1015–1027, https://doi.org/10.1101/gad.1402406.

[74] C. Verna, S.J. Ravichandran, M.G. Sawchuk, N.M. Linh, E. Scarpella, Coordination of tissue cell polarity by auxin transport and signaling, Elife 8 (2019) 1–30, https://doi.org/10.7554/eLife.51061.

[75] A. Hay, M. Barkoulas, M. Tsiantis, ASYMMETRIC LEAVES1 and auxin activities converge to repress BREVIPEDICELLUS expression and promote leaf development in Arabidopsis, Development 133 (2006) 3955–3961, https://doi.org/10.1242/dev.02545.

[76] C.S. Galvan-Ampudia, M.M. Julkowska, E. Darwish, J. Gandullo, R.A. Korver, G. Brunoud, M.A. Haring, T. Munnik, T. Vernoux, C. Testerink, Halotropism is a response of plant roots to avoid a saline environment, Curr. Biol. 23 (2013) 2044–2050, https://doi.org/10.1016/j.cub.2013.08.042.

[77] M. Zwiewka, T. Nodzyński, S. Robert, S. Vanneste, J. Friml, Osmotic stress modulates the balance between exocytosis and clathrin-mediated endocytosis in Arabidopsis thaliana, Mol. Plant 8 (2015) 1175–1187, https://doi.org/10.1016/j.molp.2015.03.007.

[78] W. Liu, R.-J. Li, T.-T. Han, W. Cai, Z.-W. Fu, Y.-T. Lu, Salt stress reduces root meristem size by nitric oxide-mediated modulation of auxin accumulation and signaling in Arabidopsis, Plant Physiol. 168 (2015) 343–356, https://doi.org/10.1104/pp.15.00030.

[79] J.I. Kim, D. Baek, H.C. Park, H.J. Chun, D.-H. Oh, M.K. Lee, J.-Y. Cha, W.-Y. Kim, M.C. Kim, W.S. Chung, H.J. Bohnert, S.Y. Lee, R.A. Bressan, S.-W. Lee, D.-J. Yun, Overexpression of Arabidopsis YUCCA6 in potato results in high-auxin developmental phenotypes and enhanced resistance to water deficit, Mol. Plant 6 (2013) 337–349, https://doi.org/10.1093/mp/sss100.

[80] Q. Ke, Z. Wang, C.Y. Ji, J.C. Jeong, H.-S. Lee, H. Li, B. Xu, X. Deng, S.-S. Kwak, Transgenic poplar expressing Arabidopsis YUCCA6 exhibits auxin-overproduction phenotypes and increased tolerance to abiotic stress, Plant Physiol. Biochem. 94 (2015) 19–27, https://doi.org/10.1016/j.plaphy.2015.05.003.

[81] P. Marhava, L. Hoermayer, S. Yoshida, P. Marhavý, E. Benková, J. Friml, Re-activation of stem cell pathways for pattern restoration in plant wound healing, Cell 177 (2019) 957–969, https://doi.org/10.1016/j.cell.2019.04.015, e13.

[82] T. Vernoux, J. Kronenberger, O. Grandjean, P. Laufs, J. Traas, PIN-FORMED 1 regulates cell fate at the periphery of the shoot apical meristem, Development 127 (2000) 5157–5165.

[83] D. Reinhardt, T. Mandel, C. Kuhlemeier, Auxin regulates the initiation and radial position of plant lateral organs, Plant Cell 12 (2000) 507–518, https://doi.org/10.1105/tpc.12.4.507.

[84] D. Reinhardt, E.R. Pesce, P. Stieger, T. Mandel, K. Baltensperger, M. Bennett, J. Traas, J. Friml, C. Kuhlemeier, Regulation of phyllotaxis by polar auxin transport, Nature. 426 (2003) 255–260, https://doi.org/10.1038/nature02081.

[85] M. Furutani, Y. Nakano, M. Tasaka, MAB4-induced auxin sink generates local auxin gradients in Arabidopsis organ formation, Proc. Nat. Acad. Sci. U. S. A 2013 (2013), https://doi.org/10.1073/pnas.1316109111.

[86] M.G. Heisler, C. Ohno, P. Das, P. Sieber, G.V. Reddy, J.A. Long, E.M. Meyerowitz, Patterns of auxin transport and gene expression during primordium development revealed by live imaging of the Arabidopsis inflorescence meristem, Curr. Biol. 15 (2005) 1899–1911, https://doi.org/10.1016/j.cub.2005.09.052.

[87] F. Besnard, Y. Refahi, V. Morin, B. Marteaux, G. Brunoud, P. Chambrier, F. Rozier, V. Mirabet, J. Legrand, S. Lainé, E. Thévenon, E. Farcot, C. Cellier, P. Das, A. Bishopp, R. Dumas, F. Parcy, Y. Helariutta, A. Boudaoud, C. Godin, J. Traas, Y. Guédon, T. Vernoux, Cytokinin signalling inhibitory fields provide robustness to phyllotaxis, Nature 505 (2014) 417–421, https://doi.org/10.1038/nature12791.

[88] T. Berleth, T. Sachs, Plant morphogenesis: long-distance coordination and local patterning, Curr. Opin. Plant Biol. 4 (2001) 57–62, https://doi.org/10.1016/S1369-5266(00)00136-9.

[89] K. Wabnik, J. Kleine-Vehn, J. Balla, M. Sauer, S. Naramoto, V. Reinöhl, R.M. H. Merks, W. Govaerts, J. Friml, Emergence of tissue polarization from synergy of intracellular and extracellular auxin signaling, Mol. Syst. Biol. 6 (2010), https://doi.org/10.1038/msb.2010.103.

[90] M. Glanc, M. Fendrych, J. Friml, Mechanistic framework for cell-intrinsic re-establishment of PIN2 polarity after cell division, Nat. Plants 4 (2018) 1082–1088, https://doi.org/10.1038/s41477-018-0318-3.

[91] N. Geldner, J. Firml, Y.D. Stierhof, G. Jürgens, K. Palme, Auxin transport inhibitors block PIN1 and vessicle trafficking, Nature 413 (2001) 425–428.

[92] I.A. Paponov, J. Dindas, E. Król, T. Friz, V. Budnyk, W. Teale, M. Paponov, R. Hedrich, K. Palme, Auxin-induced plasma membrane depolarization is regulated by AUXIN transport and not by AUXIN BINDING PROTEIN1, Front. Plant Sci. 9 (2019), https://doi.org/10.3389/fpls.2018.01953.

[93] R. Hertel, K.S. Thomson, V.E.A. Russo, In-vitro auxin binding to particulate cell fractions from corn coleoptiles, Planta 107 (1972) 325–340, https://doi.org/10.1007/BF00386394.

[94] M. Löbler, D. Klämbt, Auxin-binding protein from coleoptile membranes of corn (Zea mays L.). II. Localization of a putative auxin receptor, J. Biol. Chem. 260 (1985) 9854–9859.

[95] Y. Effendi, S. Rietz, U. Fischer, G.F.E. Scherer, The heterozygous abp1/ABP1 insertional mutant has defects in functions requiring polar auxin transport and in regulation of early auxin-regulated genes, Plant J. 65 (2011) 282–294, https://doi.org/10.1111/j.1365-313X.2010.04420.x.

[96] N. Braun, J. Wyrzykowsk, P. Muller, K. David, D. Couch, C. Perrot-Rechenmann, A.J. Fleming, Conditional repression of Auxin Binding Protein1 reveals that it coordinates cell division and cell expansion during postembryonic shoot development in Arabidopsis and tobacco, Plant Cell 20 (2008) 2746–2762, https://doi.org/10.1105/tpc.108.059048.

[97] A. Tromas, S. Paque, V. Stierlé, A.L. Quettier, P. Muller, E. Lechner, P. Genschik, C. Perrot-Rechenmann, Auxin-Binding Protein 1 is a negative regulator of the SCF TIR1/AFB pathway, Nat. Commun. 4 (2013), https://doi.org/10.1038/ncomms3496.

[98] A.M. Jones, Auxin-dependent cell expansion mediated by overexpressed auxin-binding protein 1, Science (80-.) 282 (1998) 1114–1117, https://doi.org/10.1126/science.282.5391.1114.

[99] J.M. Bauly, I.M. Sealy, H. Macdonald, J. Brearley, S. Droge, S. Hillmer, D. G. Robinson, M.A. Venis, M.R. Blatt, C.M. Lazarus, R.M. Napier, Overexpression of auxin-binding protein enhances the sensitivity of guard cells to auxin, Plant Physiol. 124 (2000) 1229–1238, https://doi.org/10.1104/pp.124.3.1229.

[100] K. Palme, T. Hesse, N. Campos, C. Garbers, M.F. Yanofsky, J. Schell, Molecular analysis of an auxin binding protein gene located on chromosome 4 of arabidopsis, Plant Cell 4 (1992) 193–201, https://doi.org/10.1105/tpc.4.2.193.

[101] W. Diekmann, M.A. Venis, D.G. Robinson, Auxins induce clustering of the auxin-binding protein at the surface of maize coleoptile protoplasts, Proc. Natl. Acad. Sci. U. S. A. 92 (1995) 3425–3429, https://doi.org/10.1073/pnas.92.8.3425.

[102] R.M. Napier, K.M. David, C. Perrot-Rechenmann, A short history of auxin-binding proteins, Plant Mol. Biol. 49 (2002) 339–348.

[103] J.M. Dunwell, J.G. Gibbings, T. Mahmood, S.M. Saqlan Naqvi, Germin and germin-like proteins: evolution, structure, and function, Crit. Rev. Plant Sci. 27 (2008) 342–375, https://doi.org/10.1080/07352680802333938.